

First Principles Nonadiabatic Excited-State Molecular Dynamics in NWChem

Huajing Song,^{*,∇} Sean A. Fischer,^{*,∇} Yu Zhang, Christopher J. Cramer, Shaul Mukamel, Niranjana Govind,^{*} and Sergei Tretiak^{*}

 Cite This: *J. Chem. Theory Comput.* 2020, 16, 6418–6427

 Read Online

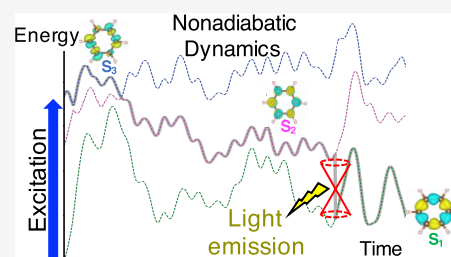
ACCESS |

 Metrics & More

 Article Recommendations

 Supporting Information

ABSTRACT: Computational simulation of nonadiabatic molecular dynamics is an indispensable tool for understanding complex photoinduced processes such as internal conversion, energy transfer, charge separation, and spatial localization of excitons, to name a few. We report an implementation of the fewest-switches surface-hopping algorithm in the NWChem computational chemistry program. The surface-hopping method is combined with linear-response time-dependent density functional theory calculations of adiabatic excited-state potential energy surfaces. To treat quantum transitions between arbitrary electronic Born–Oppenheimer states, we have implemented both numerical and analytical differentiation schemes for derivative nonadiabatic couplings. A numerical approach for the time-derivative nonadiabatic couplings together with an analytical method for calculating nonadiabatic coupling vectors is an efficient combination for surface-hopping approaches. Additionally, electronic decoherence schemes and a state reassigned unavoided crossings algorithm are implemented to improve the accuracy of the simulated dynamics and to handle trivial unavoided crossings. We apply our code to study the ultrafast decay of photoexcited benzene, including a detailed analysis of the potential energy surface, population decay timescales, and vibrational coordinates coupled to the excitation dynamics. We also study the photoinduced dynamics in trans-distyrylbenzene. This study provides a baseline for future implementations of higher-level frameworks for simulating nonadiabatic molecular dynamics in NWChem.



1. INTRODUCTION

Nonadiabatic dynamics^{1–3} generally defines the evolution of electronic excitations in optically active materials. It is commonly associated with a number of fundamental and complex processes such as intraband relaxation,⁴ energy transfer,⁵ and light harvesting⁶ influenced by the spatial evolution of excitations, and transformation of photoexcitation energy into electrical energy via charge separation.⁷ Such nonequilibrium molecular dynamics typically involves a complex manifold of intersecting excited electronic states, where the Born–Oppenheimer approximation breaks down since the electronic and nuclear timescales are comparable.⁸ A quantitative treatment of these processes typically requires computationally expensive high-level electronic structure methods in the combined electronic and nuclear space.^{9,10} Here, we employ a mixed quantum-classical dynamics approach,¹¹ which provides a reasonable compromise between computational cost and accuracy allowing treatment of realistic molecular systems.^{8,12–14}

Molecular dynamics with quantum transitions (MDQT),^{15,16} particularly the fewest-switches surface-hopping (FSSH) approach,¹⁷ is a well-tested method for simulating nonadiabatic dynamics. In spite of its *ad hoc* formulation, the success of FSSH has been previously demonstrated in a wide range of systems.^{8,11–13,18–22} In the surface-hopping approach,

an ensemble of trajectories is propagated, wherein each trajectory nuclei evolve along the adiabatic/diabatic potential energy surface (PES) of the current electron state. Nuclei are treated classically, while electrons are treated quantum mechanically, and transitions (hops) among coupled electronic states incorporate feedback between the electronic and nuclear subsystems. At the single trajectory level, detailed insights into mechanistic information can be gained, while observables such as excited-state lifetimes and energy or charge transfer rates are obtained from averages over many trajectories. The statistical ensemble of trajectories used in surface-hopping algorithms allows quantum yields²³ and branching ratios²⁴ to be determined quantitatively.

Here, we report an implementation of first-order state-to-state nonadiabatic derivative couplings and multistate nonadiabatic molecular dynamics (NAMMD)² using a combination of linear-response time-dependent density functional theory (LR-TDDFT)^{9,10,25–27} and FSSH to study and analyze

Received: March 26, 2020

Published: August 18, 2020



photochemical transformations^{28,29} in the NWChem computational chemistry package.^{30,31} All required gradients and couplings are computed simultaneously within the LR-TDDFT framework. In addition, two electronic decoherence schemes, instantaneous decoherence correction (IDC)³² and energy-based decoherence correction (EDC),^{33,34} have also been implemented together with the FSSH method to improve the accuracy of the simulated dynamics. Finally, with the addition of the state reassignment algorithm³⁵ to identify instances of unavoided crossings between noninteracting potential energy surfaces, our NAMD implementation can also handle trivial unavoided crossings,³⁶ which are common in large molecular systems.

The rest of the paper is organized as follows. In Section 2, we briefly review the basic working equations of the FSSH method, the IDC and EDC electronic decoherence schemes, and the algorithm to identify crossing events, respectively. Our NAMD implementation is described in Section 3. In Section 4, we present and discuss the results of our simulations of photoexcited dynamics of benzene, including a detailed analysis of the potential energy surface, population decay timescales, and vibrational coordinates coupled to the excitation dynamics. To further illustrate our SH-NAMD implementation, we present a study of the photoinduced dynamics in trans-distyrylbenzene in Section 5. We present our conclusions and outlook in Section 6.

2. THEORETICAL METHODOLOGY

To model the nonradiative relaxation of molecular systems, we have implemented the FSSH method of Tully¹⁷ in NWChem,^{30,31} building on our previous implementation of *ab initio* molecular dynamics³⁷ in NWChem and our extensive experience developing NAMD in the NEXMD program.^{4,6,38} FSSH is one of the most popular nonadiabatic dynamics methods and has shown reliable accuracy across a variety of different problems, including a recent examination of its accuracy for condensed-phase simulations.^{5,8,12,39} The central idea of FSSH is to approximate quantum dynamics through an ensemble of classical trajectories. Each trajectory is independent and restricted to evolve on a single adiabatic potential energy surface (PES) at any time; however, the trajectory is allowed to make transitions between electronic states subject to conditions that will be explained below. The population dynamics of the system are then determined by counting the number of trajectories on a given state at a given time.

2.1. Fewest-Switches Surface Hopping. We give a brief overview of the FSSH approach and refer the reader to the published literature for more detailed discussions.^{17,40–42} The initial molecular geometry is typically prepared by a finite-temperature ground-state trajectory. After excitation to a desired electronic state, the evolution of the nuclear degrees of freedom continues along the excited-state potential energy surface $E_n(\mathbf{R})$ according to Newton's equations of motion

$$M \frac{d^2 \mathbf{R}}{dt^2} = -\nabla_{\mathbf{R}} E_n(\mathbf{R}) \quad (1)$$

where M is the nuclear mass, \mathbf{R} represents the nuclear coordinates, and $E_n = E_0 + \Omega_n$ is the energy of the n th electronic state (E_0 and Ω_n represent the ground-state energy and the n th state excitation energy). To determine which electronic state the trajectory should follow, the time-

dependent electronic Schrödinger equation is propagated alongside the classical equation of motion

$$i\hbar \frac{\partial \Theta(\mathbf{r}, \mathbf{R}, t)}{\partial t} = \hat{H}_{\text{el}}(\mathbf{r}, \mathbf{R}) \Theta(\mathbf{r}, \mathbf{R}, t) \quad (2)$$

where \mathbf{r} represents the electronic coordinates and \hat{H}_{el} is the electronic Hamiltonian. The total electronic wave function Θ is expanded in a set of electronic basis functions

$$\Theta(\mathbf{r}, \mathbf{R}, t) = \sum_n c_n(t) \Psi_n(\mathbf{r}, \mathbf{R}) \quad (3)$$

eq 2 can be recast in terms of elements of the density matrix by defining

$$a_{nm}(t) = c_n(t) c_m^*(t) \quad (4)$$

thereby yielding

$$i\hbar \frac{d(a_{nm}(t))}{dt} = \sum_l \{ a_{lm}(t) [V_{nl}(\mathbf{R}) - i\hbar \dot{\mathbf{R}} \cdot \mathbf{d}_{nl}(\mathbf{R})] - a_{nl}(t) [V_{lm}(\mathbf{R}) - i\hbar \dot{\mathbf{R}} \cdot \mathbf{d}_{lm}(\mathbf{R})] \} \quad (5)$$

where

$$V_{nl}(\mathbf{R}) = \langle \Psi_n(\mathbf{r}, \mathbf{R}) | \hat{H}_{\text{el}}(\mathbf{r}, \mathbf{R}) | \Psi_l(\mathbf{r}, \mathbf{R}) \rangle_{\mathbf{r}} = E_l - E_n \quad (6)$$

which is diagonal in the adiabatic basis with $V_{nn} = E_n$. Finally

$$\mathbf{d}_{nm}(\mathbf{R}) = \langle \Psi_n(\mathbf{r}, \mathbf{R}) | \nabla_{\mathbf{R}} \Psi_m(\mathbf{r}, \mathbf{R}) \rangle_{\mathbf{r}} \quad (7)$$

is the nonadiabatic coupling vector (NACR).

In the present implementation, we propagate eq 1 via velocity Verlet and eq 5 via fourth-order Runge–Kutta⁴³ algorithms, respectively. Density functional theory (DFT) and LR-TDDFT are used to evaluate the electronic energies and nonadiabatic couplings. We have implementations for both full LR-TDDFT/RPA^{25,27} and the Tamm–Dancoff approximation (TDA)⁴⁴ to LR-TDDFT (See the Supporting Information (SI) Section 1). The time-dependent nonadiabatic coupling elements (NACT)

$$\dot{\mathbf{R}} \cdot \mathbf{d}_{nm} = \langle \Psi_n | \frac{\partial}{\partial t} \Psi_m \rangle \quad (8)$$

are calculated using the pseudo-wave-function approach^{12,45} and the numerical scheme of Ryabinkin and co-workers,¹³ which uses the finite-difference approximation at the level of the molecular orbitals rather than the Slater determinants (see the SI Section 2). This numerical scheme results in essentially the same values for the couplings as the analytic derivative scheme described below, but can be orders of magnitude faster.

Equation 8 calculates the coupling element NACT ($\dot{\mathbf{R}} \cdot \mathbf{d}_{nm}$, where $\dot{\mathbf{R}}$ is the velocity of the nuclei) directly with a numerical scheme. To maintain the conservation of the total electron-nuclear energy when the state is changed, the component of the nuclear velocities in the direction of the nonadiabatic coupling (NACR) must be rescaled. To that end, the NACR vector $\mathbf{d}_{nm}(\mathbf{R})$ from eq 7 is needed. We have implemented in NWChem⁴⁶ the approach developed by Send and co-workers⁴⁷ and Parker and co-workers¹² based on the analytical LR-TDDFT excitation energy gradients formalism of Furche and Ahlrichs.⁴⁸ The first-order derivative coupling between the ground and an excited electronic state, within the adiabatic approximation, is obtained from a pole analysis of the frequency-dependent linear response of the time-dependent Kohn–Sham wave function^{47,49} and expressed as

$$\mathbf{d}_{0n}^{(\xi)} = [\langle \mathbf{D}^{0n, \text{AO}} \mathbf{h}^{(\xi)} \rangle + \langle \mathbf{D}^{0n, \text{AO}} \mathbf{v}^{\text{xc}, (\xi)} \rangle - \langle \mathbf{W}^{0n, \text{AO}} \mathbf{S}^{(\xi)} \rangle + \langle \mathbf{\Gamma}^{0n, \text{AO}} \mathbf{V}^{(\xi)} \rangle] \cdot \Omega_n^{-1} \quad (9)$$

where the superscript (ξ) indicates partial differentiation with respect to the nuclear coordinate of interest, the superscript AO indicates quantities expressed in the atomic orbital basis, where an arbitrary matrix \mathbf{M} in the MO representation can be transformed to the AO representation as $\mathbf{M}^{\text{AO}} = \mathbf{C}\mathbf{M}\mathbf{C}^*$ using the molecular orbital coefficient matrix \mathbf{C} . \mathbf{h} is the one-electron core Hamiltonian, \mathbf{v}^{xc} is the exchange–correlation potential, \mathbf{S} is the AO overlap matrix, \mathbf{D}^{0n} is a generalized one-electron transition density, \mathbf{W}^{0n} is a generalized energy-weighted transition density, $\mathbf{\Gamma}^{0n}$ is the pair transition density, and \mathbf{V} is the two-electron Coulomb operator defined by $V_{\mu\nu\lambda\kappa} = (\mu\nu|\lambda\kappa)$; greek indices denote AOs. Further details are given in SI Section 3 and refs 12, 47

In analogy with the ground-to-excited state derivative coupling, the state-to-state NACR between excited states n and m can be written as

$$\mathbf{d}_{nm}^{(\xi)} = [\langle \mathbf{D}^{nm, \text{AO}} \mathbf{h}^{(\xi)} \rangle + \langle \mathbf{D}^{nm, \text{AO}} \mathbf{v}^{\text{xc}, (\xi)} \rangle - \langle \mathbf{W}^{nm, \text{AO}} \mathbf{S}^{(\xi)} \rangle + \langle \mathbf{\Gamma}^{nm, \text{AO}} \mathbf{V}^{(\xi)} \rangle + \langle \mathbf{\Gamma}^{nm, \text{AO}} \mathbf{f}^{\text{xc}, (\xi)} \rangle] \cdot \Omega_{nm}^{-1} \quad (10)$$

where \mathbf{D}^{nm} and $\mathbf{\Gamma}^{nm}$ are the one-electron and pair transition density matrices, $f_{\mu\nu\lambda\kappa}^{\text{xc}}$ represents a matrix element of the exchange–correlation kernel in the adiabatic approximation, $\Omega_{nm} = \Omega_n - \Omega_m$ is the energy difference between excited states n and m , and all other quantities are defined as in eq 9. Further details about the construction of density matrices \mathbf{D}^{nm} , \mathbf{W}^{nm} , and $\mathbf{\Gamma}^{nm}$ can be found in SI Section 3 and ref 12.

The FSSH algorithm allows the system to hop to another adiabatic state at any time t , and the probability that the nuclear trajectory will hop from the electronic state n to some other state m during the time interval Δt is

$$g_{n \rightarrow m}(\mathbf{R}, t) = \Delta t \cdot \frac{b_{mn}(\mathbf{R}, t)}{a_{nn}(t)} \quad (11)$$

$$b_{mn}(\mathbf{R}, t) = 2\hbar^{-1} \text{Im}(a_{nm}^*(t) V_{nm}(\mathbf{R})) - 2 \text{Re}(a_{nm}^*(t) \dot{\mathbf{R}} \cdot \mathbf{d}_{nm}(\mathbf{R})) \quad (12)$$

According to eq 4, $a_{nn}(t) = c_n^*(t) c_n(t)$ and the quantity $b_{mn}(\mathbf{R}, t)$ is related to the probability flux $\dot{a}_{nn}(t) = \sum_{j \neq k} b_{jk}(\mathbf{R}, t)$. Note that $g_{n \rightarrow m} = -g_{m \rightarrow n}$ and $g_{n \rightarrow n} = 0$, since $\mathbf{d}_{nm} = -\mathbf{d}_{mn}$ and $\mathbf{d}_{nn} = \mathbf{0}$.⁴ Hopping probabilities less than zero are set to zero. During the dynamics, ground to excited state transition density matrices should be monitored and maintained with the same phase (sign) to avoid a sudden sign change in the nonadiabatic coupling. This is done by modifying the phases so that the largest component of each solution vector remains positive along the trajectory.

At each time step, the hopping probabilities from the current state to all other states are calculated and a uniform random number, ζ , on the interval (0,1) is selected. A transition from the current state n to state m occurs if

$$\sum_{\substack{l=1 \\ l \neq n}}^m g_{n \rightarrow l} < \zeta \leq \sum_{\substack{l=1 \\ l \neq n}}^{m+1} g_{n \rightarrow l} \quad (13)$$

Finally, if $\sum_{l \neq n}^{l=1} g_{n \rightarrow l} < \zeta > 1$, then the system remains in state n .

To evaluate the nuclear and electronic degrees of freedom during the molecular dynamics simulations, analytic excited-state gradients are calculated $-\nabla_{\mathbf{R}} E_n(\mathbf{R})$, which are used for propagating the nuclei geometry according to Newton's equations of motion eq 1. The electronic energies $E_n(\mathbf{R})$ and NACT couplings $\dot{\mathbf{R}} \cdot \mathbf{d}_{nm}$ are updated at every trajectory point $\mathbf{R}(t)$ with the atomic time step Δt . However, the time variations of the real and imaginary parts of the quantum coefficients in eq 5 require a smaller time step $\delta t \leq \Delta t$. Therefore, the atomic interval Δt is split up into N_q time steps with $\delta t = \Delta t/N_q$. Then, eq 1 is propagated via the fourth-order Runge–Kutta method with smaller time steps $t + n \delta t$ ($n = 0, \dots, N_q - 1$), with a simple linear interpolation and extrapolation scheme to obtain the electronic energies E_n and NACT couplings $\dot{\mathbf{R}} \cdot \mathbf{d}_{nm}$. The switching probabilities, $g_{n \rightarrow b}$, are recast in terms of the integral over time steps

$$g_{n \rightarrow m}(\mathbf{R}, t) = \frac{\int_t^{t+N_q \delta t} dt b_{mn}(\mathbf{R}, t)}{a_{nn}(t)} \quad (14)$$

where $N_q = \Delta t/\delta t$ is the number of electronic steps per atomic integration step. The composite Simpson's rule was used to perform the numerical integration in eq 14.

After a hop, the nuclear trajectory begins to evolve in a new state, and the components of the nuclear velocities along the direction of the nonadiabatic coupling vectors¹⁵ (\mathbf{d}_{0n} from eq 9 or \mathbf{d}_{nm} from eq 10) are rescaled to conserve the total electron–nuclear energy. If a hop to an electronic state of higher energy is predicted and the kinetic energy available in the nuclear coordinates along the direction of the nonadiabatic coupling is insufficient, the hop is rejected. The velocity adjustment procedure has been discussed elsewhere in detail.⁵⁰ Ultimately, velocity rescaling and hop rejection create a detailed balance between transitions to higher and lower energy.⁵¹

2.2. Electronic Decoherence. In the standard FSSH formulation, eq 5 is integrated throughout the trajectory, leading to coherences between electronic states that persist long after the trajectory has left the coupling region.³² These coherences are unphysical and can potentially cause numerical problems (i.e., violation of internal consistency of the algorithm³²). Several decoherence corrections have been suggested in the literature. In this work, we have implemented two electronic decoherence algorithms: the instantaneous decoherence correction (IDC)³² and the energy-based decoherence correction (EDC).^{33,34}

The IDC³² is based on the assumption that divergent wave packets will instantly separate in-phase space and should immediately undergo independent evolution. Once a hop has occurred, the IDC procedure reinitializes the quantum coefficients to one for the new current state, while the populations for all other states are set to zero. After resetting the coefficients, the standard coefficient evolution according to eq 5 once again takes over and the wave packet again broadens until another hopping event happens, at which point the process of resetting the coefficients will be repeated. Thus, the wave packet undergoes a series of broadening and collapsing events mediated by the trajectory hopping. In this way, after each hop, the center of the wave packet is realigned with the current state and internal consistency is restored. In our current implementation, the IDC is active in all attempted hops. If the hop is successful, the coefficient of the new state will be set to one and the system will begin evolving on the new state. If the hop is forbidden, the coefficient of the old

state is set to one and the system will continue evolving on the old state.

The EDC scheme, on the other hand, relies on rescaling the quantum coefficients after each classical time step. The electronic wave function is repeatedly initialized as a pure state, and coefficient evolution is governed by eq 5. However, the wave packet is not permitted to undergo a natural broadening. After each nuclear time step, the coefficients are rescaled (damped) and the wave packet is narrowed before continuing the evolution using the rescaled values. Following Granucci and Persico,^{33,34} rescaling is performed according to the following protocol $\forall m \neq n$, where n denotes the current state

$$a'_{lm} = a_{lm} \exp\left\{\frac{-\Delta t(\tau_{nl} + \tau_{nm})}{\tau_{nl}\tau_{nm}}\right\} \quad \forall m, l \neq n \quad (15)$$

$$a'_{nm} = a_{nm} \exp\left\{\frac{-\Delta t}{\tau_{nm}}\right\} \left[\frac{1 - \sum_{l \neq n} a_{ll}}{a_{nn}}\right]^{1/2} \quad (16)$$

$$a'_{nn} = 1 - \sum_{l \neq n} a'_{ll} \quad (17)$$

$$\tau_{nm} = \frac{\hbar}{|E_n - E_m|} \left(1 + \frac{C_{\text{EDC}}}{E_{\text{kin}}}\right) \quad (18)$$

where C_{EDC} is a constant, which we set to 0.1 Hartree, in line with previous work^{33,34,52,53} and E_{kin} is the nuclear kinetic energy.

The current implemented decoherence corrections are similar to the NEXMD implementation,^{6,8,32,38} which has been fully verified for semiempirical Hamiltonian models. Both IDC and EDC decoherence corrections add almost no computational cost and have been shown to give good results for the population dynamics.³² The IDC provides a simple method of including decoherence in nonadiabatic molecular dynamics simulations. The results improve internal consistency while at the same time providing a result that does not depend on external parameters and maintains physical relevance. On the other hand, the EDC is more reliable for systems with small energy gaps in the spectrum.³² However, the EDC may be dependent on the parameters chosen, which can be significant for some systems.³² Currently, the IDC is the default option in our implementation in NWChem.

2.3. Trivial Unavoided Crossings. In excited-state molecular dynamics, either weakly or strongly avoided crossings as well as unavoidable crossings are common events during radiationless vibronic relaxation.^{54–56} Conical intersections dominate nonadiabatic nuclear dynamics on the very short (femtosecond) timescales.² In extended polyatomic molecules, special cases of unavoidable crossings can also take place between two noninteracting states in the same energy range.^{36,57} In such cases, denoted accidental unavoidable crossings, the nonadiabatic couplings behave as sharp peaks strongly localized at the exact crossing points and vanish elsewhere. Here, the wave packet trajectory must cross the conical intersection seam following the diabatic pathway of its parent wave function along the respective adiabatic PES. Failure to follow the correct pathway can lead to unphysical sudden changes in the spatial localization of the current state.⁵⁸

We have implemented the algorithm of Fernandez-Alberti and co-workers³⁶ to identify crossing events by tracking the

identities of states over time. Using the Min-Cost assignment algorithm,^{35,59} new states at the current time step i can be assigned in terms of old states at the preceding time step $(i - 1)$. The correspondence between states is found at each time step based on maximizing the trace of the square of the overlap matrix, S , whose elements are given by

$$s_{nm}(t; t + \Delta t) \equiv \langle \Psi_m(t) | \Psi_n(t + \Delta t) \rangle \\ = \sum_{\mu, \nu} \rho^{0m}(t)_{\mu\nu} \cdot \rho^{0n}(t + \Delta t)_{\nu\mu} \quad (19)$$

where Ψ_n and Ψ_m are the adiabatic electronic state wave functions, \mathbf{r} and \mathbf{R} represent electronic and nuclear coordinates, respectively, and Δt is the classical time step used for the LR-TDDFT/TDA simulations. This is done by selecting one element from each row, each pertaining to a different column (or vice versa), of the matrix $\mathbf{R}(t + \Delta t)$ such that the sum of their squared values is maximized. For a maximum overlap greater than a threshold, states are reassigned by interchanging their populations, ignoring their couplings and the hopping probability is not evaluated for the unavoided crossings states. The dependence of the non-adiabatic coupling strength on the proximity to the exact crossing point is thus removed by construction. Unavoided crossings involving interacting states (simulated by quantum hops) can then be differentiated from trivial unavoidable crossings between noninteracting states (detected by tracking state identities). The current treatment of trivial unavoidable crossings is similar to the NEXMD implementation, further details and verification of the method are provided in refs 36, 38, 57

3. NAMD IMPLEMENTATION

We have implemented the FSSH nonadiabatic molecular dynamics (NAMD) as an extension to the quantum molecular dynamics (QMD) module³⁷ in NWChem. The workflow is as follows: For each timestep, a ground-state DFT calculation is first performed. This is followed by a LR-TDDFT/RPA or TDA calculation to compute the excitation energies Ω_s and configuration interaction (CI) vectors. Excited-state forces are calculated using LR-TDDFT/RPA or TDA gradients, and derivative couplings are determined using the pseudo-wavefunction approach.⁴⁵

To start the NAMD simulation, we initiate classical trajectories as in *ab initio* molecular dynamics (AIMD). Preparation of the initial conditions (snapshots of the molecular geometry \mathbf{R} with the respective set of nuclear velocities $\dot{\mathbf{R}}$) is a critical preliminary step in the simulations. The initial sampling of the conformational space should be adequate to represent the equilibrated ensemble of molecules at the given thermodynamic conditions, which may be achieved using different thermostat models. Some possible options for the thermostat in NWChem are stochastic velocity rescaling,⁶⁰ Langevin dynamics,⁶¹ Nosé–Hoover thermostats,⁶² Berendsen thermostat,⁶³ and velocity rescaling (*i.e.*, isokinetic ensemble⁶⁴). In the current study, a stochastic velocity rescaling thermostat⁶⁰ is applied to achieve the canonical ensemble for the initial sampling. Depending on the molecular system, the snapshots can be taken every 1–10 ps after the molecule has been equilibrated in the ground state for 10–50 ps. This allows the initialization of nuclear coordinates \mathbf{R} and velocities $\dot{\mathbf{R}}$ from these snapshots to form a wave packet for the excited-state NAMD simulations. The

next step is to populate the initial excited states. The number of propagated excited states, M_{eff} , should be sufficiently large to include possible upward hops to higher-energy states. The subsequent NAMD simulations can be run either at constant energy or constant temperature. Here, we use the stochastic velocity rescaling thermostat to maintain a canonical ensemble during the NAMD stage. The inclusion of a thermostat is critical to achieve appropriate ground-state conformational sampling. A suitable thermostat relaxation timescale can prevent unphysical high-temperature fluctuations during the equilibrium process, which may adversely affect the SCF/TDDFT convergence. However, an overly small relaxation time will over-restrict the atomic motion, thus precluding the system reaching equilibrium. The thermostat relaxation time has to be larger than the atomic scale and should relate to the system size and the target temperature. The default thermostat relaxation time is ~ 1000 a.u. Typically, the thermostat has a smaller effect on the electronic energy relaxation rates in ultrafast nonradiative excited-state dynamics (See ref 65).

After assigning the initial conditions, the NAMD algorithm calculates each trajectory as follows:

1. Propagate nuclei in the interval $t \rightarrow t + \Delta t$ along the n th electronic state. The gradient of the currently occupied state $-\nabla_{\mathbf{R}} E_n(\mathbf{R})$, along with the energies of all adiabatic electronic states $E_m = E_0 + \Omega_m$ and the NACT couplings between all pairs of states $\dot{\mathbf{R}} \cdot \mathbf{d}_{nm}$ are evaluated at each timestep t .
2. Check the trivial unavoided crossing based on the Min-Cost assignment algorithm. If a trivial crossing is detected, the states are reassigned by interchanging their populations and setting their couplings $\dot{\mathbf{R}} \cdot \mathbf{d}_{nm} = 0$ and the hopping probability is not evaluated for those states involved in the trivial crossing.
3. Propagate the quantum coefficients $a_{nm}(t)$ according to eq 5 at the N_q intervals $[t + n \delta t, t + (n + 1) \delta t]$ ($n = 0, \dots, N_q - 1$). The state energies E_m and NACT couplings, $\dot{\mathbf{R}} \cdot \mathbf{d}_{nm}$ (eq 8), are obtained via a linear interpolation assumption at each quantum interval $t + n \delta t$.
4. Evaluate the switching probabilities, g_{mn} (eq 14), using the NACT $\dot{\mathbf{R}} \cdot \mathbf{d}_{nm}$ values computed using eq 8. Generate a random number and determine whether a switch to another potential energy surface is needed using eq 13. If a hop $n \rightarrow m$ is realized, the velocities are adjusted, and the nuclei propagate on the m th state.
5. The IDC decoherence correction is invoked only when a hop is realized. On the other hand, the EDC decoherence correction, if used, is computed at each atomic step following the evaluation of the switching probabilities.
6. If a successful hop is confirmed, the state energy and gradient will be updated in the newly occupied state.
7. Store relevant data and return to step (1).

4. EXCITED-STATE NONRADIATIVE RELAXATION OF BENZENE

To validate and demonstrate our implementation, we have studied the photoinduced dynamics of benzene in the gas phase. The dynamics simulation was initiated by first optimizing the molecule in the singlet ground state. This was followed by a 10 ps DFT-MD trajectory at 300 K with a time step of 10 a.u. (~ 0.2419 fs). The stochastic velocity rescaling thermostat⁶⁰ was applied with a relaxation time of 800 a.u.

After a 5 ps equilibration period, 100 snapshots were randomly sampled from the second half of the trajectory and served as starting points for the SH-NAMD runs. Typically, the excited system will hop downwards to lower states from the initial state. However, to account for possible upward hops, one has to include 1–2 excited states above the initial state in the FSSH algorithm. We have included a total of four excited states ($S_{1,\dots,4}$), and all NAMD runs were initiated on the bright S_3 excited state. All excited states were computed within LR-TDDFT/TDA approximation, with SCF convergence thresholds set to $10^{-8} E_h$. In total, we have simulated 100 independent trajectories with a 10 ps simulation time for each trajectory. We ran three sets of calculations with different exchange–correlation functionals and basis sets (PBE0⁶⁶/STO-3G,⁶⁷ PBE0/Def2-SVP,⁶⁸ and B3LYP⁶⁹/Def2-SVP) to compare our results. We also ran our trajectories with a smaller 5 a.u. (~ 0.121 fs) time step. A sample of the input file for NAMD simulation of water is given in the SI Section 5.

On timescales below ~ 1 ps, internal conversion in molecules typically involves excited electronic states only. Nonradiative and radiative transitions to the ground state usually occur on much longer (nanosecond) timescales. Hereafter, we focus on dynamics spanning the $S_{1,\dots,4}$ excited state manifold. Notably, as mentioned in other published works,^{12,70} conical intersections between the ground state and an excited state have incorrect dimensionality with LR-TDDFT⁷¹ due to Brillouin's theorem.⁷² This calls for the use of alternative approaches.^{28,73–75}

The two lowest-lying excited states of benzene (S_1 and S_2) are $\pi-\pi^*$ transitions. S_1 is an optically forbidden transition, dominated by a (HOMO-1) \rightarrow LUMO transition. S_2 is a bright $\pi-\pi^*$ transition noticeable in the absorption spectra and dominated by a HOMO \rightarrow LUMO orbital transition. The third excited-state (S_3), on the other hand, is a bright $\sigma-\pi^*$ transition mostly characterized by a single (HOMO-2) \rightarrow LUMO transition. Table 1 shows the dependence of the vertical excitation energies on exchange–correlation functional and basis.

Table 1. Comparison of the Vertical Excitation Energies for the First Three Singlet Excited States of Benzene and Relaxation Lifetime of $S_2 \rightarrow S_1$ and $S_3 \rightarrow S_2$ Decays by Different Exchange–Correlation Functionals and Basis Sets

method	S_1 (eV)	S_2 (eV)	S_3 (eV)	$S_{2,1}$ (fs)	$S_{3,2}$ (fs)
PBE0/STO-3g	6.41	8.12	8.84	77	8.3
PBE0/Def2-SVP	5.67	6.81	7.76	57	11
B3LYP/Def2-SVP	5.32	6.31	7.10	61	9.1

Figure 1 shows a typical trajectory from a SH-NAMD simulation. The dark solid line represents the active trajectory path. Upon initiation on the S_3 state, benzene rapidly undergoes internal conversion to S_2 within ~ 50 fs. In most cases, the $S_3 \rightarrow S_2$ transition is enabled by surface hopping. However, as shown in Figure 1, the first crossing at ~ 22 fs is a typical trivial unavoided crossing involving the S_3 and S_2 surfaces, which the Min-Cost assignment algorithm^{35,59} effectively identified thus allowing for the treatment of trivial unavoided crossings between weakly or noninteracting adiabatic states. The second crossing at ~ 81 fs is an example of surface hopping: the quantum transition between electronic states S_2 and S_1 depends on their nonadiabatic coupling strength.

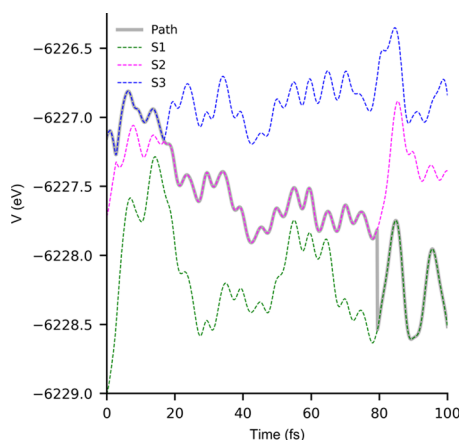


Figure 1. Example trajectory showing the internal conversion $S_3 \rightarrow S_2 \rightarrow S_1$ over a span of 100 fs.

Figure 2 compares the evolution of the excited-state populations along the ensemble of trajectories. A small number

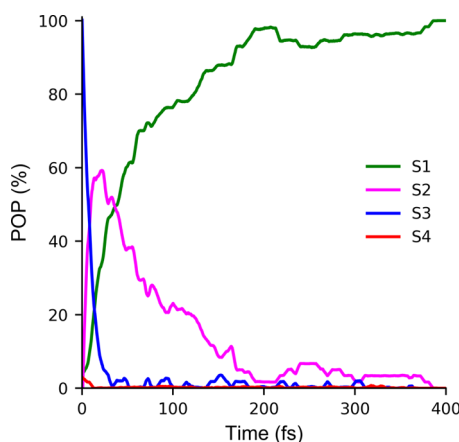


Figure 2. Excited-state populations evaluated over trajectory swarms using PBE0/Def2-SVP.

(4 out of 100) of upward hoppings to S_4 is observed at the start of the dynamics. Excited-state populations in **Figure 2** were calculated as $p_k(t) = N_k(t)/N_{\text{traj}}$, where $N_k(t)$ is the number of trajectories with state k being the active state at time t . The detailed nonadiabatic dynamics are expected to be highly sensitive to the energy difference between different excited states, and this is clearly reflected in the half-life of each state. Referring to the vertical excitation energies in **Table 1**, we find the S_3 decay to be significantly faster than the other states due to the smaller S_3 – S_2 energy gap. With PBE0/Def2-SVP, 90% of the S_3 state population decays in the first ~ 50 fs. As a comparison, the S_2 – S_1 transition occurs at longer timescales up to ~ 180 fs due to the larger S_2 – S_1 energy gap. The simulated rates for the two electronic decays ($S_3 \rightarrow S_2$ and $S_{n(n=3,2)} \rightarrow S_1$) are characterized as single exponential decays from which lifetimes are defined respectively according to¹²

$$p_3(t > 0) \approx e^{-t/\tau_3} \quad (20)$$

and

$$p_1(t > 0) \approx 1 - e^{-t/\tau_1} \quad (21)$$

where τ_3 corresponds to the S_3 – S_2 transition and τ_1 corresponds to the rise of the S_1 state lifetime. τ_3 is estimated through the S_3 half-life, $t_{S_3,1/2} = 8$ fs, according to

$$\tau_3 = t_{S_3,1/2}/\ln 2 \quad (22)$$

while τ_1 is similarly estimated from the final value in the simulation using

$$\tau_1 = -t_f/\ln(1 - p_{1,f}) \quad (23)$$

where t_f and $p_{1,f} = p_1(t_f)$ are the time and population used to estimate the rate.

Using the set of PBE0/Def2-SVP simulations, we find the S_3 lifetime to be $\tau_3 \sim 11$ fs which agrees well (to within a factor of 0.5) with the 20 fs lifetimes measured by experiment. Consequently, we assign the prompt signal to the S_3 – S_2 decay. The total $S_{n(n=3,2)}$ – S_1 excited state lifetime was found to be ~ 57 fs, which is also within the uncertainty range 70 ± 30 fs lifetimes measured by pump–probe experiments⁷⁶ for the rise of S_1 state population in benzene.

Table 1 also lists the relaxation times corresponding to $S_3 \rightarrow S_2$ and $S_2 \rightarrow S_1$ decays calculated for different exchange–correlation functionals and basis sets. The S_3 lifetime for PBE0/STO-3g and B3LYP/Def2-SVP are 8.3 and 9.1 fs, respectively. Comparing to the S_3 lifetime 11 fs of PBE0/Def2-SVP, the observed increased rate can be attributed to the reduced energy gap at the Franck–Condon geometry between S_3 and S_2 states, $\Delta E_{32} = E_3 - E_2$, which is 0.72 eV at PBE0/STO-3g and 0.79 eV at B3LYP/Def2-SVP. Corresponding to the 0.95 eV at PBE0/Def2-SVP, the energy gap and the S_3 lifetime both reduce by $\sim 76\%$ for PBE0/STO-3g and $\sim 83\%$ for B3LYP/Def2-SVP. The relaxation rate thus shows a strong dependence on the gaps between different electronic states in the same functional/basis or between different functional/basis sets.

We next analyze the intramolecular vibrational energy redistribution. **Figure 3** shows the following benzene bond lengths that are monitored as a function of time over the course of the dynamics. C–H is the carbon hydrogen bond length, C–C1 and C–C2 are the hybrid bonds on the two sides of the carbon atoms in the ring, and the ring puckering amplitude, Q , computed using the Cremer–Pople coordinates,⁷⁷ which measures the deviation of atoms from the mean plane of the ring ($Q = 0$). Immediately after excitation to S_3 , both of the hybrid bonds C–C1 and C–C2 experience a sudden increase. The bonds then undergo an ultrafast relaxation that follows the $S_3 \rightarrow S_2 \rightarrow S_1$ electronic energy transfer (**Figure 2**). Since in our simulations there is no decay to the ground state (S_0), larger values of C–C bond lengths are obtained than that in the ground state. The C–H bond shows no significant difference between ground and excited states. This suggests that most of the vibrational energy is released from the C–C hybrid bonds in the ring. In addition, the puckering amplitude is more than three times the equilibrium value of ~ 0.03 – ~ 0.09 Å within 50 fs. However, based on the geometry optimized structures, ground-state and excited-state benzene should have a similar flat six-membered ring, and thus the increased degree of puckering can be attributed to the increased dynamical vibrational energy resulting from the nonradiative decay.

The initial localization of the transition density (orbital representation of diagonal element of \mathbf{D}^{0j} in eq 9) is shown in **Figure 4** for the PBE0/Def2-SVP optimized planar ground-

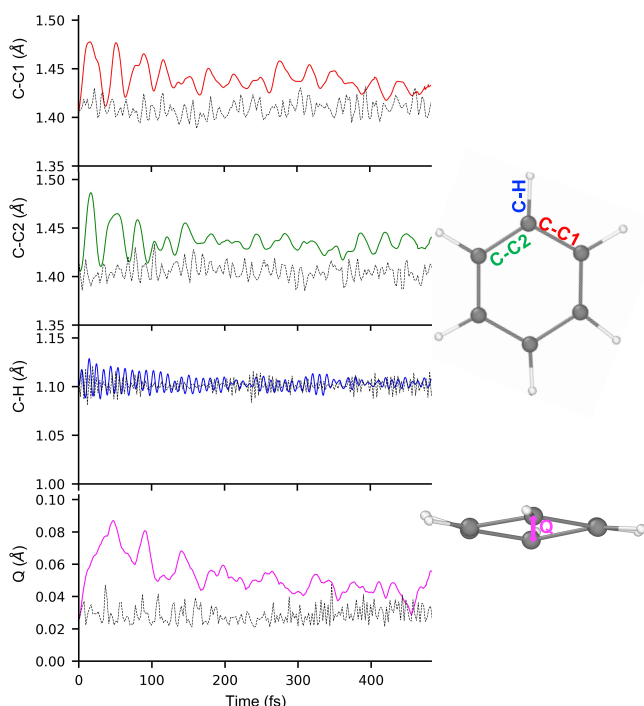


Figure 3. Geometrical properties measured over trajectory swarms accompanying ultrafast NAMD simulated with PBE0/Def2-SVP. The solid lines correspond to trajectories that undergo electronic energy transfer, and the dashed lines are from trajectories on the ground state.

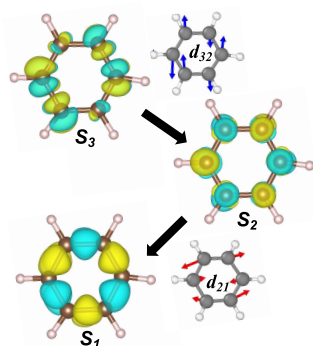


Figure 4. Volumetric plots of the transition densities for the three excited states S_3 , S_2 , and S_1 at the ground-state equilibrium geometry and the corresponding nonadiabatic coupling vectors (\mathbf{d}_{32} and \mathbf{d}_{21}) during the transition.

state geometry, which reflects the spatial distributions of the excited-state wave functions. The electronic density during $S_3 \rightarrow S_2 \rightarrow S_1$ transition is concomitant with an excess vibrational energy released to C–C bonds. This further agrees with the nonadiabatic coupling vectors \mathbf{d}_{32} and \mathbf{d}_{21} , which are all localized on the ring. Moreover, the $S_2 \rightarrow S_1$ transition is a typical out-of-phase orbital to in-phase orbital transition, which reflects “+” and “−” wave function combinations as discussed by Nelson and co-workers.⁵ This is also consistent with previous studies,^{5,7} \mathbf{d}_{21} vectors have the corresponding spatially asymmetric characteristic, conveying the vibrational excitation

dynamically emerging due to electronic transition, in the form of compression and expansion.

Table 2 shows CPU times for each calculation in an SH-NAMD timestep of Benzene using the PBE0 functional and

Table 2. CPU Timings (in Unit of Second) for an SH-NAMD Timestep of Benzene with PBE0/Def2-SVP^a

calculation	CPU times (s)
TDDFT	19.7
NACT	0.1
NACR	2.9
PES update	20.0

^aTests were performed on the Badger computer system with 36 Intel Xeon Processors E5-2695 v4 (45M Cache, 2.10 GHz).

Def2-SVP basis set (114 basis functions). As expected, electronic structure calculation (*i.e.*, TDDFT energy and excited-state gradients) is the most time-consuming step with the NACT evaluation adding a minor cost at each atomic timestep. The NACR values are only evaluated at the suspected surface-hopping steps, which is less than 0.1% of the total timesteps. Only if a successful hop is realized, the PES needs to be updated by repeating the TDDFT in the new occupied state. Therefore, the numerical expense for the NACR and PES updates is minor, compared to the entire simulation time.

5. PHOTOINDUCED DYNAMICS IN DISTYRYLBENZENE

To further demonstrate our new implementation, we have applied our implementation to model the photoinduced dynamics of a trans-distyrylbenzene, which is a small three-ring oligomer of polyphenylene vinylene (PPV). Similar to the benzene example, the PPV system was equilibrated in the ground state for 5 ps at 300 K, then 20 independent NAMD trajectories were initiated on the S_3 excited state with the PBE0 functional and STO-3G basis set. Figure 5a shows a single trajectory potential energy of the three lowest energy states

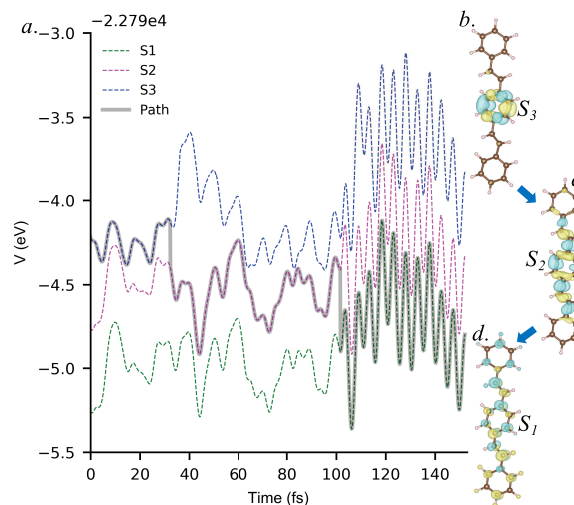


Figure 5. (a) is an example of PPV trajectory that shows the internal conversion $S_3 \rightarrow S_2 \rightarrow S_1$ over a span of 140 fs. (b)–(d) show the excitation energy dispersal revealed by the transition density during the SH-NAMD.

during the first 140 fs of dynamics. Two typical surface-hopping events take place, ~ 36 and ~ 107 fs, indicating the $S_3 \rightarrow S_2$ and $S_2 \rightarrow S_1$ transfers. A strong vibrational excitation in all three potential energy profiles is observed right after the second hop, showing electronic energy transfer into nuclei motions. To illustrate the concomitant electronic dynamics, Figure 5b–d shows the transition density plots for states S_1 – S_3 . The energy transfer can be seen by following the dynamics of this quantity. The transition density initially localized on the central ring at S_3 , expands to the two side rings through the C=C bond bridge at S_2 , and finally getting fully delocalized to all three rings at S_1 .

6. CONCLUSIONS

We have presented our NAMD implementation in NWChem, which includes state-to-state derivative couplings and surface hopping, enabling multistate nonadiabatic molecular dynamics simulations using LR-TDDFT. Additionally, we have implemented electronic decoherence schemes and a state reassigned unavoided crossings algorithm to improve the accuracy of the dynamics and to handle trivial unavoided crossings. To demonstrate and validate our implementation, we have simulated the photoinduced dynamics in benzene and trans-distyrylbenzene. We note that electronic coherences and decoherences associated with nuclear wave packet overlaps are completely ignored by the surface-hopping approach, which was formulated to treat population dynamics phenomenologically. These effects are essential for the simulation of ultrafast nonlinear optical and X-ray coherent signals. To this end, we are extending our current framework to include multiconfigurational Ehrenfest *ab initio* multiple cloning (MCE-AIMC)⁷⁸ that will be suitable for simulating ultrafast spectroscopic spectra.^{79–82}

■ ASSOCIATED CONTENT

Supporting Information

The Supporting Information is available free of charge at <https://pubs.acs.org/doi/10.1021/acs.jctc.0c00295>.

Brief review of linear-response TDDFT; nonadiabatic coupling element (NACT); nonadiabatic coupling vector (NACR); testing of the nonadiabatic coupling calculation; example NWChem input (PDF)

■ AUTHOR INFORMATION

Corresponding Authors

Huajing Song – *Physics and Chemistry of Materials, Theoretical Division, Los Alamos National Laboratory, Los Alamos, New Mexico 87545, United States*; orcid.org/0000-0001-5958-7377; Email: songhw@lanl.gov

Sean A. Fischer – *Chemistry Division, U.S. Naval Research Laboratory, Washington, District of Columbia 20375, United States*; orcid.org/0000-0003-2242-6654; Email: sean.fischer@nrl.navy.mil

Niranjan Govind – *Physical and Computational Sciences Directorate, Pacific Northwest National Laboratory, Richland, Washington 99352, United States*; orcid.org/0000-0003-3625-366X; Email: niri.govind@pnnl.gov

Sergei Tretiak – *Physics and Chemistry of Materials, Theoretical Division and Center for Integrated Nanotechnologies, Los Alamos National Laboratory, Los Alamos, New Mexico 87545, United States*; orcid.org/0000-0001-5547-3647; Email: serg@lanl.gov

Authors

Yu Zhang – *Physics and Chemistry of Materials, Theoretical Division, Los Alamos National Laboratory, Los Alamos, New Mexico 87545, United States*; orcid.org/0000-0001-8938-1927

Christopher J. Cramer – *Department of Chemistry, Supercomputing Institute and Chemical Theory Center, University of Minnesota, Minneapolis, Minnesota 55455, United States*; orcid.org/0000-0001-5048-1859

Shaul Mukamel – *Departments of Chemistry, and physics and astronomy, University of California, Irvine, California 92697, United States*; orcid.org/0000-0002-6015-3135

Complete contact information is available at: <https://pubs.acs.org/doi/10.1021/acs.jctc.0c00295>

Author Contributions

[†]H.S. and S.A.F. contributed equally to this work.

Notes

The authors declare no competing financial interest.

■ ACKNOWLEDGMENTS

H.S., S.T., N.G., and S.M. acknowledge support from the U.S. Department of Energy, Office of Science, Basic Energy Sciences, Chemical Sciences, Geosciences, and Biosciences Division under Contracts No. KC0301030, KC030103172684, and award no. DE-SC0019484. S.T. acknowledges the support of the Center for Integrated Nanotechnology (CINT) at Los Alamos National Laboratory (LANL), a U.S. Department of Energy and Office of Basic Energy Sciences User Facility. S.A.F. acknowledges support from the U.S. Office of Naval Research through the U.S. Naval Research Laboratory. S.A.F., N.G., and C.J.C. also acknowledge support by the U.S. Department of Energy, Office of Science, Office of Advanced Scientific Computing Research, Scientific Discovery through Advanced Computing (SciDAC) program (2013–2017) under Award Nos. KC030102062653 (S.A.F. and N.G.) and DESC0008666 (C.J.C.) (Charge Transfer and Charge Transport in Photoactivated Systems), a University of Minnesota/LBNL/PNNL partnership, under which this NAMD implementation in NWChem was initially begun. This research used resources provided by the LANL Institutional Computing Program and also benefited from computational resources provided by EMSL, a DOE Office of Science User Facility sponsored by the Office of Biological and Environmental Research and located at the Pacific Northwest National Laboratory (PNNL). PNNL is operated by Battelle Memorial Institute for the United States Department of Energy under DOE contract number DE-AC05-76RL1830.

■ REFERENCES

- (1) Yarkony, D. R. Diabolical conical intersections. *Rev. Mod. Phys.* **1996**, *68*, 985.
- (2) Domcke, W.; Yarkony, D. R. Role of Conical Intersections in Molecular Spectroscopy and Photoinduced Chemical Dynamics. *Annu. Rev. Phys. Chem.* **2012**, *63*, 325–352.
- (3) Baer, M. *Beyond Born–Oppenheimer: Electronic Nonadiabatic Coupling Terms and Conical Intersections*; John Wiley & Sons, 2006.
- (4) Nelson, T.; Fernandez-Alberti, S.; Chernyak, V.; Roitberg, A.; Tretiak, S. Nonadiabatic Excited-State Molecular Dynamics Modeling of Photoinduced Dynamics in Conjugated Molecules. *J. Phys. Chem. B* **2011**, *115*, 5402–5414.
- (5) Nelson, T.; Ondarse-Alvarez, D.; Oldani, N.; Rodriguez-Hernandez, B.; Alfonso-Hernandez, L.; Galindo, F. J.; Kleiman, D.

- V.; Fernandez-Alberti, S.; Roitberg, A.; Tretiak, S. Coherent exciton-vibrational dynamics and energy transfer in conjugated organics. *Nat. Commun.* **2018**, *9*, No. 2316.
- (6) Nelson, T.; Fernandez-Alberti, S.; Roitberg, A.; Tretiak, S. Nonadiabatic Excited-State Molecular Dynamics: Modeling Photo-physics in Organic Conjugated Materials. *Acc. Chem. Res.* **2014**, *47*, 1155–1164.
- (7) Soler, M. A.; Nelson, T.; Roitberg, A.; Tretiak, S.; Fernandez-Alberti, S. Signature of Nonadiabatic Coupling in Excited-State Vibrational Modes. *J. Phys. Chem. A* **2014**, *118*, 10372–10379.
- (8) Nelson, T. R.; White, J. A.; Bjorgaard, A. J.; Sifain, E. A.; Zhang, Y.; Nebgen, B.; Fernandez-Alberti, S.; Mozyrsky, D.; Roitberg, A.; Tretiak, S. Non-adiabatic Excited State Molecular Dynamics: theory and applications for modeling photophysics in extended molecular materials. *Chem. Rev.* **2020**, *120*, 2215–2287.
- (9) Baer, R. Non-adiabatic couplings by time-dependent density functional theory. *Chem. Phys. Lett.* **2002**, *364*, 75–79.
- (10) Baer, R.; Kurzweil, Y.; Cederbaum, L. S. Time-dependent density functional theory for nonadiabatic processes. *Isr. J. Chem.* **2005**, *45*, 161–170.
- (11) Crespo-Otero, R.; Barbatti, M. Recent advances and perspectives on nonadiabatic mixed quantum–classical dynamics. *Chem. Rev.* **2018**, *118*, 7026–7068.
- (12) Parker, S.; Roy, S.; Furche, F. Multistate hybrid time-dependent density functional theory with surface hopping accurately captures ultrafast thymine photodeactivation. *J. Chem. Theory Comput.* **2018**, *14*, 807–819.
- (13) Ryabinkin, I.; Nagesh, J.; Izmaylov, F. Fast Numerical Evaluation of time-Derivative Nonadiabatic Couplings for Mixed Quantum-Classical Methods. *J. Phys. Chem. Lett.* **2015**, *6*, 4200–4203.
- (14) Akimov, A. V.; Neukirch, A. J.; Prezhdo, O. V. Theoretical Insights into Photoinduced Charge Transfer and Catalysis at Oxide Interfaces. *Chem. Rev.* **2013**, *113*, 4496–4565.
- (15) Hammes-Schiffer, S.; Tully, J. C. Proton transfer in solution: Molecular dynamics with quantum transitions. *J. Chem. Phys.* **1994**, *101*, 4657–4667.
- (16) Worth, G. A.; Robba, M. A.; Lasorne, B. Solving the Time-Dependent Schrödinger Equation for Nuclear Motion in One Setp: Direct Dynamics of Non-Adiabatic Systems. *Mol. Phys.* **2008**, *106*, 2077–2019.
- (17) Tully, J. C. Molecular Dynamics with Electronic Transitions. *J. Chem. Phys.* **1990**, *93*, 1061–1071.
- (18) alexvakimov; Smith, B.; Sato, K.; Li, W.; Sun, X.; Chan, M. *Quantum-Dynamics-Hub/Libra-Code: First Official Indexed Release*, 2019.
- (19) Richter, M.; Marquetand, P.; González-Vázquez, J.; Sola, I.; González, L. SHARC: *ab Initio* Molecular Dynamics with Surface Hopping in the Adiabatic Representation Including Arbitrary Couplings. *J. Chem. Theory Comput.* **2011**, *7*, 1253–1258.
- (20) Hammes-Schiffer, S. Hydrogen tunneling and protein motion in enzyme reactions. *Acc. Chem. Res.* **2006**, *39*, 93–100.
- (21) Antol, I.; Eckert-Maksic, M.; Barbatti, M.; Lischka, H. Simulation of the photodeactivation of formamide in the n_0 - π^* and π - π^* states: An *ab initio* on-the-fly surface-hopping dynamic study. *J. Chem. Phys.* **2007**, *127*, No. 234303.
- (22) Prezhdo, O. V. Photoinduced dynamics in semiconductor quantum dots: insights from time-domain *ab initio* studies. *Acc. Chem. Res.* **2009**, *42*, 2005–2016.
- (23) Neukirch, A. J.; Shamberger, L. C.; Abad, E.; Haycock, B. J.; Wang, H.; Ortega, J.; Prezhdo, O. V.; Lewis, J. P. Nonadiabatic ensemble simulations of cis-stilbene and cis-azobenzene photo-isomerization. *J. Chem. Theory Comput.* **2014**, *10*, 14–23.
- (24) Subotnik, J. E.; Shenoi, N. A new approach to decoherence and momentum rescaling in the surface hopping algorithm. *J. Chem. Phys.* **2011**, *134*, No. 024105.
- (25) Casida, M. E.; Huix-Rotllant, M. Progress in time-dependent density-functional theory. *Ann. Rev. Phys. Chem.* **2012**, *63*, 287–323.
- (26) Gross, E. K. U.; Dobson, J. F.; Petersilka, M. *Density Functional Theory II*; Springer-Verlag: Berlin/Heidelberg, 1996; pp 81–172.
- (27) Ullrich, C. A. *Time-Dependent Density-Functional Theory: Concepts and Applications*; Oxford University Press: Oxford, 2011.
- (28) Tapavicza, E.; Bellchambers, G. D.; Vincent, J. C.; Furche, F. *Ab Initio* non-adiabatic molecular dynamics. *Phys. Chem. Chem. Phys.* **2013**, *15*, 18336–18348.
- (29) Craig, C. F.; Duncan, W. R.; Prezhdo, O. V. Trajectory Surface Hopping in the Time-Dependent Kohn-Sham Approach for Electron-Nuclear Dynamics. *Phys. Rev. Lett.* **2005**, *95*, No. 163001.
- (30) Valiev, M.; Bylaska, E. J.; Govind, N.; Kowalski, K.; Straatsma, T. P.; van Dam, H. J. J.; Wang, D.; Nieplocha, J.; Apra, E.; Windus, T. L.; de Jong, W. A. NWChem: A Comprehensive and Scalable Open-Source Solution for Large Scale Molecular Simulations. *Comput. Phys. Commun.* **2010**, *181*, 1477–1489.
- (31) Apra, E.; Bylaska, E. J.; De Jong, W. A.; Govind, N.; Kowalski, K.; Straatsma, T. P.; Valiev, M.; van Dam, H.; Alexeev, Y.; Anchell, J.; et al. NWChem: Past, present, and future. *J. Chem. Phys.* **2020**, *152*, No. 184102.
- (32) Nelson, T.; Fernandez-Alberti, S.; Roitberg, A.; Tretiak, S. Nonadiabatic excited-state molecular dynamics: Treatment of electronic decoherence. *J. Chem. Phys.* **2013**, *138*, 224111–224124.
- (33) Granucci, G.; Persico, M.; Zocante, A. Including quantum decoherence in surface hopping. *J. Chem. Phys.* **2010**, *133*, 134111–134120.
- (34) Granucci, G.; Persico, M. Critical appraisal of the fewest switches algorithm for surface hopping. *J. Chem. Phys.* **2007**, *126*, 134114–134125.
- (35) Kalstein, A.; Fernandez-Alberti, S.; Bastida, A.; Soler, M. A.; Farag, M. H.; Zuniga, J.; Requena, A. Vibrational dynamics of polyatomic molecules in solution: assignment, time evolution and mixing of instantaneous normal modes. *Theor. Chem. Acc.* **2011**, *128*, 769–782.
- (36) Fernandez-Alberti, S.; Roitberg, A. E.; Nelson, T.; Tretiak, S. Identification of unavoided crossings in nonadiabatic photoexcited dynamics involving multiple electronic states in polyatomic conjugated molecules. *J. Chem. Phys.* **2012**, *137*, No. 014512.
- (37) Fischer, S. A.; Ueltschi, T. W.; El-Khoury, P. Z.; Mifflin, A. L.; Hess, W. P.; Wang, H.-f.; Cramer, C. J.; Govind, N. Infrared and Raman Spectroscopy from *Ab Initio* Molecular Dynamics and Static Normal Mode Analysis: The CH Region of DMSO as a Case Study. *J. Phys. Chem. B* **2016**, *120*, 1429.
- (38) Malone, W.; Nebgen, B.; White, A.; Zhang, Y.; Song, H.; Bjorgaard, J.; Sifain, A.; Rodriguez-Hernandez, B.; Freixas, V.; Fernandez-Alberti, S.; Roitberg, E.; Nelson, R.; Tretiak, S. NEXMD Software Package for Non-adiabatic Excited State Molecular Dynamics Simulations. *J. Chem. Theory Comput.* **2020**, DOI: 10.1021/acs.jctc.0c00248. (Accepted)
- (39) Chen, H.-T.; Reichman, D. R. On the Accuracy of Surface Hopping Dynamics in Condensed Phase Non-Adiabatic Problems. *J. Chem. Phys.* **2016**, *144*, No. 094104.
- (40) Tully, J. C. Mixed Quantum-Classical Dynamics. *Faraday Discuss.* **1998**, *110*, 407–419.
- (41) Jasper, A. W.; Stechmann, S. N.; Truhlar, D. G. Fewest-Switches with Time Uncertainty: A Modified Trajectory Surface-Hopping Algorithm with Better Accuracy for Classically Forbidden Electronic Transitions. *J. Chem. Phys.* **2002**, *116*, 5424–5431.
- (42) Jasper, A. W.; Truhlar, D. G. Improved Treatment of Momentum at Classically Forbidden Electronic Transitions in Trajectory Surface Hopping Calculations. *Chem. Phys. Lett.* **2003**, *369*, 60–67.
- (43) Yaakub, A. R.; Evans, D. J. A fourth order Runge–Kutta RK(4,4) method with error control. *Int. J. Comput. Math.* **1999**, *71*, 383–411.
- (44) Hirata, S.; Head-Gordon, M. Time-dependent density functional theory within the Tamm-Dancoff approximation. *Chem. Phys. Lett.* **1999**, *314*, 291–299.
- (45) Ou, Q.; Bellchambers, G. D.; Furche, F.; Subotnik, J. E. First-Order Derivative Couplings between Excited States from Adiabatic TDDFT Response Theory. *J. Chem. Phys.* **2015**, *142*, No. 064114.

- (46) Silverstein, D. W.; Govind, N.; Van Dam, H. J.; Jensen, L. Simulating one-photon absorption and resonance Raman scattering spectra using analytical excited state energy gradients within time-dependent density functional theory. *J. Chem. Theory Comput.* **2013**, *9*, 5490–5503.
- (47) Send, R.; Furche, F. First-order nonadiabatic couplings from time-dependent hybrid density functional response theory: Consistent formalism, implementation, and performance. *J. Chem. Phys.* **2010**, *132*, 44107–44119.
- (48) Furche, F.; Ahlrichs, R. Adiabatic Time-Dependent Density Functional Methods for Excited State Properties. *J. Chem. Phys.* **2002**, *117*, 7433–7447.
- (49) Li, Z.; Suo, B.; Liu, W. First-Order Nonadiabatic Coupling Matrix Elements Between Excited States: Implementation and Application at the TD-DFT and pp-TDA Levels. *J. Chem. Phys.* **2014**, *141*, 244105.
- (50) Fabiano, E.; Keal, T. W.; Thiel, W. Implementation of surface hopping molecular dynamics using semiempirical methods. *Chem. Phys.* **2008**, *349*, 334–437.
- (51) Parandekar, P. V.; Tully, J. C. Mixed Quantum-Classical Equilibrium. *J. Chem. Phys.* **2005**, *122*, No. 094102.
- (52) Zhu, C.; Nangia, S.; Jasper, A. W.; Truhlar, D. G. Coherent switching with decay of mixing: An improved treatment of electronic coherence for non-Born–Oppenheimer trajectories. *J. Chem. Phys.* **2004**, *121*, 7658–7670.
- (53) Hack, M. D.; Truhlar, D. G. A natural decay of mixing algorithm for non-Born–Oppenheimer trajectories. *J. Chem. Phys.* **2001**, *114*, 9305–9314.
- (54) Kim, M. H.; Shen, L.; Tao, L. H.; Martinez, T. J.; Suits, A. G. Conformationally Controlled Chemistry: Excited-State Dynamics Dictate Ground-State Reaction. *Science* **2007**, *315*, 1561–1565.
- (55) Scholes, G. D.; Fleming, G. R.; Olaya-Castro, A.; van Grondelle, R. Lessons from nature about solar light harvesting. *Nat. Chem.* **2011**, *3*, 763–774.
- (56) Collini, E.; Scholes, G. D. Coherent Intrachain Energy Migration in a Conjugated Polymer at Room Temperature. *Science* **2009**, *323*, 369–373.
- (57) Nelson, T.; Fernandez-Alberti, S.; Roitberg, A. E.; Tretiak, S. Artifacts due to trivial unavoided crossings in the modeling of photoinduced energy transfer dynamics in extended conjugated molecules. *Chem. Phys. Lett.* **2013**, *590*, 208–231.
- (58) Worth, G. A.; Robba, M. A.; Burghardt, I. A novel algorithm for non-adiabatic direct dynamics using variational Gaussian wavepackets. *Faraday Discuss.* **2004**, *127*, 307–323.
- (59) Carpaneto, G.; Martello, S.; Toth, P. Algorithms and codes for the assignment problem. *Ann. Oper. Res.* **1988**, *13*, 191–223.
- (60) Bussi, G.; Donadio, D.; Parrinello, M. Canonical sampling through velocity rescaling. *J. Chem. Phys.* **2007**, *126*, No. 014101.
- (61) Bussi, G.; Parrinello, M. Accurate sampling using Langevin dynamics. *Phys. Rev. E* **2007**, *75*, No. 056707.
- (62) Blöchl, P. E.; Parrinello, M. Adiabaticity in first-principles molecular dynamics. *Phys. Rev. B* **1992**, *45*, 9413.
- (63) Berendsen, H. J. C.; Postma, J. P. M.; van Gunsteren, W. F.; Di Nola, A.; Haak, J. R. Molecular dynamics with coupling to an external bath. *J. Chem. Phys.* **1984**, *81*, 3684–3690.
- (64) Omelyan, I.; Kovalenko, A. Generalised canonical–isokinetic ensemble: speeding up multiscale molecular dynamics and coupling with 3D molecular theory of solvation. *Mol. Simul.* **2013**, *39*, 25–48.
- (65) Shenai, P. M.; Fernandez-Alberti, S.; Bricker, W. P.; Tretiak, S.; Zhao, Y. Internal Conversion and Vibrational Energy Redistribution in Chlorophyll A. *J. Phys. Chem. B* **2016**, *120*, 49–58.
- (66) Adamo, C.; Barone, V. Toward reliable density functional methods without adjustable parameters: The PBE0 model. *J. Chem. Phys.* **1999**, *110*, 6158–6170.
- (67) Collins, J. B.; Schleyer, P. vR.; Binkley, J. S.; A, P. J. Self-Consistent Molecular Orbital Methods. 17. Geometries and binding energies of second-row molecules. A comparison of three basis sets. *J. Chem. Phys.* **1976**, *64*, 5142–5151.
- (68) Weigend, F.; Ahlrichs, R. Balanced Basis Sets of Split Valence, Triple Zeta Valence and Quadruple Zeta Valence Quality for H to Rn: Design and Assessment of Accuracy. *Phys. Chem. Chem. Phys.* **2005**, *7*, 3297–3305.
- (69) Becke, A. D. Density-functional thermochemistry. V. Systematic optimization of exchange-correlation functionals. *J. Chem. Phys.* **1997**, *107*, 8554–8561.
- (70) Stojanović, L.; Bai, S.; Nagesh, J.; Izmaylov, A. F.; Crespo-Otero, R.; Lischka, H.; Barbatti, M. New Insights into the State Trapping of UV-Excited Thymine. *Molecules* **2016**, *21*, No. 1603.
- (71) Levine, B. G.; Ko, C.; Quenneville, J.; Martinez, T. J. Conical intersections and double excitations in time-dependent density functional theory. *Mol. Phys.* **2006**, *104*, 1039–1051.
- (72) Szabo, A.; Ostlund, N. S. *Modern Quantum Chemistry: Introduction to Advanced Electronic Structure Theory*; Courier Corporation, 2012.
- (73) Li, S. L.; Marenich, A. V.; Xu, X.; Truhlar, D. G. Configuration Interaction-Corrected Tamm-Dancoff Approximation: A Time-Dependent Density Functional Method with the Correct Dimensionality of Conical Intersections. *J. Phys. Chem. Lett.* **2014**, *5*, 322–328.
- (74) Shu, Y.; Parker, K. A.; Truhlar, D. G. Dual-functional Tamm-Dancoff approximation: a convenient density functional method that correctly describes S1/S0 conical intersections. *J. Phys. Chem. Lett.* **2017**, *8*, 2107–2112.
- (75) Zhang, Y.; Li, L.; Tretiak, S.; Nelson, T. R. Non-Adiabatic Excited-State Molecular Dynamics for Open-Shell Systems. *J. Chem. Theory Comput.* **2020**, *16*, 2053–2064.
- (76) Farmanara, P.; Steinkellner, O.; Wick, M.; Wittmann, M.; Korn, G.; Stert, V.; Radloff, W. Ultrafast internal conversion and photodissociation of molecules excited by femtosecond 155 nm laser pulses. *J. Chem. Phys.* **1999**, *111*, 6264–6270.
- (77) Cremer, D.; Pople, J. A. General definition of ring puckering coordinates. *J. Am. Chem. Soc.* **1975**, *97*, 1354–1358.
- (78) Freixas, V. M.; Fernandez-Alberti, S.; Makhov, D. V.; Tretiak, S.; Shalashilin, D. An ab initio multiple cloning approach for the simulation of photoinduced dynamics in conjugated molecules. *Phys. Chem. Chem. Phys.* **2018**, *20*, 17762–17772.
- (79) Bennett, K.; Zhang, Y.; Kowalewski, M.; Hua, W.; Mukamel, S. Multidimensional resonant nonlinear spectroscopy with coherent broadband x-ray pulses. *Phys. Scr.* **2016**, *T169*, No. 014002.
- (80) Kowalewski, M.; Fingerhut, B.; Dorfman, K. E.; Bennett, K.; Mukamel, S. Simulating Coherent Multidimensional Spectroscopy of Nonadiabatic Molecular Processes; from the Infrared to the X-ray Regime. *Chem. Rev.* **2017**, *117*, 12165–12226.
- (81) Mukamel, S. *Principles of Nonlinear Optical Spectroscopy*; Oxford series in optical and imaging sciences; Oxford University Press, 1995.
- (82) Kowalewski, M.; Bennett, K.; Dorfman, K. E.; Mukamel, S. Catching Conical Intersections in the Act: Monitoring Transient Electronic Coherences by Attosecond Stimulated X-Ray Raman Signals. *Phys. Rev. Lett.* **2015**, *115*, No. 193003.

First Principles Non-Adiabatic Excited-State Molecular Dynamics in NWChem: Supporting Information

HUAJING SONG^{1,*}, SEAN A. FISCHER^{2,*}, YU ZHANG¹, CHRISTOPHER J. CRAMER³, SHAUL MUKAMEL⁴, NIRANJAN GOVIND^{5,*}, AND SERGEI TRETIAK^{1,6,*}

¹Physics and Chemistry of Materials, Theoretical Division, Los Alamos National Laboratory, Los Alamos, New Mexico, 87545, USA

²Chemistry Division, U.S. Naval Research Laboratory, Washington, DC 20375, USA

³Department of Chemistry, Supercomputing Institute and Chemical Theory Center, University of Minnesota, Minneapolis, MN 55455, USA

⁴Departments of Chemistry, and physics and astronomy, University of California, Irvine, CA 92697, USA

⁵Physical and Computational Sciences Directorate, Pacific Northwest National Laboratory, Richland, WA 99352, USA

⁶Center for Integrated Nanotechnologies, Los Alamos National Laboratory, Los Alamos, New Mexico 87545, USA

*Corresponding author: songhw@lanl.gov, sean.fischer@nrl.navy.mil, niri.govind@pnnl.gov, serg@lanl.gov.

1. BRIEF REVIEW OF LINEAR-RESPONSE TDDFT

In the linear response TDDFT (LR-TDDFT) [1], excitation energies are obtained by solving the eigenvalue problem

$$(\Lambda - \Omega_n \Delta) |X^n, Y^n\rangle = 0, \quad (\text{S1})$$

where

$$\Lambda = \begin{pmatrix} \mathbf{A} & \mathbf{B} \\ \mathbf{B} & \mathbf{A} \end{pmatrix}, \quad \Delta = \begin{pmatrix} 1 & 0 \\ 0 & -1 \end{pmatrix}. \quad (\text{S2})$$

The matrices $(\mathbf{A} + \mathbf{B})$ and $(\mathbf{A} - \mathbf{B})$ denote the electronic and magnetic orbital rotation Hessians, have the matrix representation

$$\begin{aligned} (A + B)_{ia,jb} &= \varepsilon_{ab} \delta_{ij} - \varepsilon_{ij} \delta_{ab} + 2f_{ia,jb}^{xc} + 2(ia|jb) \\ &\quad - c_x [(ib|ja) + (ij|ab)] \end{aligned} \quad (\text{S3})$$

and

$$(A - B)_{ia,jb} = \varepsilon_{ab} \delta_{ij} - \varepsilon_{ij} \delta_{ab} + c_x [(ib|ja) - (ij|ab)]. \quad (\text{S4})$$

Ω_n and $|X^n, Y^n\rangle$ are the eigenvalue (excitation energy) and associated eigenvector of excited state n respectively. Here, indices i, j, \dots denote occupied, a, b, \dots virtual, and p, q, \dots general Kohn-Sham molecular orbitals (MOs). $(pq|rs)$ is a two-electron repulsion integral in Mulliken notation. Moreover, ε_{pq} is an element of the Kohn-Sham matrix which is also known as the MOs energy, is assumed to be block-diagonal (*i.e.*, the occupied-virtual blocks vanish). $f_{pq,rs}^{xc}$ is the exchange-correlation kernel in the adiabatic approximation

$$f_{pq,rs}^{xc} = \frac{\delta^2 E^{xc}}{\delta \rho_{pq}(\mathbf{r}) \delta \rho_{rs}(\mathbf{r}')}. \quad (\text{S5})$$

E^{xc} denotes the static exchange-correlation energy functional, and c_x is a scalar that interpolates between pure semilocal density functionals ($c_x = 0$) and Hartree-Fock theory ($c_x = 1$, $f^{xc} = 0$), which is also known as the random phase approximation (RPA) for excitation energies. The configuration interaction singles (CIS) or Tamm-Dancoff approximation (TDA) easily derived by constraining Y^n identically to zero in the variation of G . To this end, we introduce a family of the single-electron density matrices defined as

$$(\rho_{nm})_{\mu\nu} = \langle \Psi_n | c_\mu^\dagger c_\nu | \Psi_m \rangle. \quad (\text{S6})$$

where $c_\mu^\dagger (c_\nu)$ are creation (annihilation) operators in atomic orbital (AO) basis, and μ, ν, \dots represent the AO basis functions. n and m label the adiabatic electronic eigenstates of the system, and $\Psi_{m/n}$ are the corresponding adiabatic wave functions. Thus, ρ_{0n} is the transition density matrix (TDM), which represents the changes in the density matrix induced by an optical transition from the ground state $|0\rangle$ to the excited state $|\Psi_n\rangle$. Upon solving the TDDFT equations, the excitation energy Ω_n and eigenvectors (sometimes called configuration interaction (CI) vectors) X^n and Y^n are all obtained. Meanwhile, these eigenvectors from Eq. S1 are subject to the orthonormalization condition [2]

$$\langle X^n, Y^n | \Delta | X^m, Y^m \rangle = \delta_{nm}, \quad (\text{S7})$$

and the transition density matrix ρ_{nm} is able to constructure from these CI vectors. More details can be found in Supporting Information (SI.3) and ref. 3-5.

2. NON-ADIABATIC COUPLING ELEMENT (NACT)

For completeness we provide the expressions for the evaluation of the non-adiabatic coupling elements within the context of single-electron excitations from a single Slater determinant reference. The NACT between states n and m is given by

$$\dot{\mathbf{R}} \cdot \mathbf{d}_{nm} = \sigma_{nm} = \left\langle \Psi_n \left| \frac{\partial}{\partial t} \Psi_m \right. \right\rangle. \quad (\text{S8})$$

We expand the states in Slater determinants,

$$|\Psi_n\rangle = C_0^n |\Phi_0\rangle + \sum_{ia} C_{ia}^n |\Phi_i^a\rangle, \quad (\text{S9})$$

again i, j, \dots represents an occupied and a, b, \dots represents a virtual in MO. Note that the coefficient C_0^n will be 1 for the ground state and 0 for any other state. Additionally, be careful not to confuse these coefficients with those of Eq. 3: the two are unrelated. We will assume real expansion coefficients as this is usually the case. Inserting the expansion into the expression for the non-adiabatic coupling element gives

$$\begin{aligned} \sigma_{nm} = & C_0^n \frac{\partial}{\partial t} C_0^m \langle \Phi_0 | \Phi_0 \rangle + C_0^n C_0^m \left\langle \Phi_0 \left| \frac{\partial}{\partial t} \Phi_0 \right. \right\rangle \\ & + \sum_{jb} \left\{ C_0^n \frac{\partial}{\partial t} C_{jb}^m \langle \Phi_0 | \Phi_j^b \rangle \right\} + \sum_{jb} \left\{ C_0^n C_{jb}^m \left\langle \Phi_0 \left| \frac{\partial}{\partial t} \Phi_j^b \right. \right\rangle \right\} \\ & + \sum_{ia} \left\{ C_{ia}^n \frac{\partial}{\partial t} C_0^m \langle \Phi_i^a | \Phi_0 \rangle \right\} + \sum_{ia} \left\{ C_{ia}^n C_0^m \left\langle \Phi_i^a \left| \frac{\partial}{\partial t} \Phi_0 \right. \right\rangle \right\} \\ & + \sum_{ia,jb} \left\{ C_{ia}^n \frac{\partial}{\partial t} C_{jb}^m \langle \Phi_i^a | \Phi_j^b \rangle \right\} + \sum_{ia,jb} \left\{ C_{ia}^n C_{jb}^m \left\langle \Phi_i^a \left| \frac{\partial}{\partial t} \Phi_j^b \right. \right\rangle \right\}. \end{aligned} \quad (\text{S10})$$

Applying the orthonormality of the Slater determinants reduces the expression to

$$\begin{aligned} \sigma_{nm} = & \sum_{jb} \left\{ C_0^n C_{jb}^m \left\langle \Phi_0 \left| \frac{\partial}{\partial t} \Phi_j^b \right. \right\rangle \right\} + \sum_{ia} \left\{ C_{ia}^n C_0^m \left\langle \Phi_i^a \left| \frac{\partial}{\partial t} \Phi_0 \right. \right\rangle \right\} \\ & + \sum_{ia} \left\{ C_{ia}^n \frac{\partial}{\partial t} C_{ia}^m \right\} + \sum_{ia,jb} \left\{ C_{ia}^n C_{jb}^m \left\langle \Phi_i^a \left| \frac{\partial}{\partial t} \Phi_j^b \right. \right\rangle \right\}. \end{aligned} \quad (\text{S11})$$

Note the first term is zero because the expansion coefficient of the ground state is time independent as a consequence of Brillouin's theorem and our restriction to only single-electron excitations from a single determinant reference. When computing the coupling elements numerically, common practice has been to apply the finite difference approximation for the time derivatives at this point. This leads to having to evaluate determinants of matrices whose elements are the overlap integrals of the molecular orbitals of the Slater determinants. This procedure scales as $N_{vir}^2 N_{occ}^5$, with N_{vir} being the number of virtual orbitals and N_{occ} being the number of occupied orbitals (N_{occ}^3 for evaluation of a single determinant and $(N_{vir} N_{occ})^2$ determinants to evaluate). This is a substantial cost, and indeed the evaluation of the coupling elements themselves can be more expensive than the rest of the computations in a time step combined, including the excited state gradient calculation.

The alternative approach used previously by some and formalized by Ryabinkin et al.[6] is to first reduce the expressions further by assuming a single set of orthonormal molecular orbitals and then apply the finite difference approximation. This reduction results in the expression for the non-adiabatic coupling elements being given by

$$\begin{aligned} \sigma_{nm} = & \sum_{ia} \left\{ C_0^n C_{ia}^m \left\langle \phi_i \left| \frac{\partial}{\partial t} \phi_a \right. \right\rangle + C_{ia}^n C_0^m \left\langle \phi_a \left| \frac{\partial}{\partial t} \phi_i \right. \right\rangle \right\} \\ & + \sum_{ia} \left\{ C_{ia}^n \frac{\partial}{\partial t} C_{ia}^m \right\} + \sum_{iab} \left\{ C_{ia}^j C_{ib}^m \left\langle \phi_a \left| \frac{\partial}{\partial t} \phi_b \right. \right\rangle \right\} - \sum_{ija} \left\{ C_{ia}^n C_{ja}^m \left\langle \phi_j \left| \frac{\partial}{\partial t} \phi_i \right. \right\rangle \right\}. \end{aligned} \quad (\text{S12})$$

The first two terms are relevant for coupling between the ground state and the excited states, while the last three terms couple the excited states to each other. The most expensive term (for typical calculations) in this expression is the fourth term, which scales as $N_{occ} N_{vir}^2$. This is a dramatic reduction in computational cost. Additionally, all of the terms in this expression can be evaluated as matrix-matrix multiplications, which can be efficiently parallelized. In our implementation the coupling evaluation adds essentially no cost to the calculation and a single surface hopping trajectory is no more expensive than an adiabatic excited state trajectory of the same length.

For orthonormal wavefunctions, the non-adiabatic coupling matrix is anti-symmetric ($\sigma_{nm} = -\sigma_{mn}^*$). In making the finite difference approximation for the derivatives, we explicitly use this anti-symmetry:

$$\sigma_{nm} = -\sigma_{mn}^* \quad (\text{S13})$$

$$\sigma_{nm} + \sigma_{mn} = \sigma_{nm} - \sigma_{mn}^* \quad (\text{S14})$$

$$2\sigma_{nm} = \sigma_{nm} - \sigma_{mn}^* \quad (\text{S15})$$

$$\sigma_{nm} = \frac{\sigma_{nm} - \sigma_{mn}^*}{2} \quad (\text{S16})$$

From this last expression and the backward difference approximation, it is straightforward to derive the following expression for the non-adiabatic couplings

$$\begin{aligned} \sigma_{nm}(t) \approx & \frac{1}{2\Delta t} \left[\sum_{ia} \{C_0^n(t)C_{ia}^m(t) [\langle \phi_i(t-\Delta t) | \phi_a(t) \rangle - \langle \phi_i(t) | \phi_a(t-\Delta t) \rangle] \} \right. \\ & + \sum_{ia} \{C_{ia}^n(t)C_0^m(t) [\langle \phi_a(t-\Delta t) | \phi_i(t) \rangle - \langle \phi_a(t) | \phi_i(t-\Delta t) \rangle] \} \\ & + \sum_{ia} \{C_{ia}^n(t-\Delta t)C_{ia}^m(t) - C_{ia}^n(t)C_{ia}^m(t-\Delta t)\} \\ & + \sum_{iab} \{C_{ia}^n(t)C_{ib}^m(t) [\langle \phi_a(t-\Delta t) | \phi_b(t) \rangle - \langle \phi_a(t) | \phi_b(t-\Delta t) \rangle] \} \\ & \left. - \sum_{ija} \{C_{ia}^n(t)C_{ja}^m(t) [\langle \phi_j(t-\Delta t) | \phi_i(t) \rangle - \langle \phi_j(t) | \phi_i(t-\Delta t) \rangle] \} \right]. \end{aligned} \quad (S17)$$

During the implementation, the time derivative MOs overlap matrix

$$S_{pq}(t, t-\Delta t) = \langle \phi_p(t) | \phi_q(t-\Delta t) \rangle, \quad (S18)$$

is calculated from the basis sets overlap and converted from atomic orbitals (AOs) to MOs by the molecular orbital coefficient matrix \mathbf{C} .

$$S_{pq}(t, t-\Delta t) = \sum_{\mu\nu} C_{\mu p}(t) \langle \phi_\mu(t) | \phi_\nu(t-\Delta t) \rangle C_{\nu q}(t-\Delta t), \quad (S19)$$

and

$$\mathbf{S}(t-\Delta t, t) = \mathbf{S}(t, t-\Delta t)^T, \quad (S20)$$

where p, q represent general MOs, μ, ν are AOs, $\langle \cdot \rangle$ indicates a trace and superscript "T" is a transpose symbol. According to the CI vectors calculated from LR-TDDFT, the Eq. S17 is implemented by two separate cases,

Ground-Excited Coupling

$$\sigma_{0m}(t) \approx \frac{1}{2\Delta t} \sum_{jb} \left\{ (X+Y)_{jb}^m [S_{bj}(t, t-\Delta t) - S_{jb}(t, t-\Delta t)] \right\}. \quad (S21)$$

Excited-Excited Coupling

$$\sigma_{nm}(t) \approx \frac{1}{2\Delta t} \left(\sigma_{nm}^{CI}(t) + \sigma_{nm}^{1MO}(t) + \sigma_{nm}^{2MO}(t) \right) \quad (S22)$$

CI derivative contribution:

$$\begin{aligned} \sigma_{nm}^{CI}(t) = & \sum_{ia} \frac{1}{2} \left\{ [(X+Y)_{ia}^n (X+Y)_{ia}^m + (X-Y)_{ia}^n (X-Y)_{ia}^m] \right. \\ & \left. - [(X+Y)_{ia}^n (X+Y)_{ia}^m + (X-Y)_{ia}^n (X-Y)_{ia}^m] \right\}, \end{aligned} \quad (S23)$$

where $(\mathbf{X} + \mathbf{Y})$ is the current timestep (t) value and $(\mathbf{X} + \mathbf{Y})'$ is the previous timestep ($t - \Delta t$) value.

1st MO derivative contribution:

$$\begin{aligned} \sigma_{nm}^{1MO}(t) = & \sum_{iab} \frac{1}{2} \left\{ [(X+Y)_{ia}^n (X+Y)_{ib}^m + (X-Y)_{ia}^n (X-Y)_{ib}^m] S_{ba}(t, t-\Delta t) \right. \\ & \left. - [(X+Y)_{ia}^n (X+Y)_{ib}^m + (X-Y)_{ia}^n (X-Y)_{ib}^m] S_{ab}(t, t-\Delta t) \right\}. \end{aligned} \quad (S24)$$

2nd MO derivative contribution:

$$\begin{aligned} \sigma_{nm}^{2MO}(t) = & \sum_{ija} \frac{1}{2} \left\{ [(X+Y)_{ia}^n (X+Y)_{ja}^m + (X-Y)_{ia}^n (X-Y)_{ja}^m] S_{ji}(t, t-\Delta t) \right. \\ & \left. - [(X+Y)_{ia}^n (X+Y)_{ja}^m + (X-Y)_{ia}^n (X-Y)_{ja}^m] S_{ij}(t, t-\Delta t) \right\}. \end{aligned} \quad (S25)$$

More details can be found in ref. 6.

3. NON-ADIABATIC COUPLING VECTOR (NACR)

Quadratic response theory dictates that the state-state transition density matrix (TDM) is obtained from [4]

$$\rho^{nm,QR} = \begin{pmatrix} -(\mathbf{X}^n(\mathbf{X}^m)^T + \mathbf{Y}^n(\mathbf{Y}^m)^T) & \mathbf{X}^{nm} \\ \mathbf{Y}^{nm} & (\mathbf{X}^n)^T\mathbf{X}^m + (\mathbf{Y}^n)^T\mathbf{Y}^m \end{pmatrix} \quad (\text{S26})$$

where the off-diagonal blocks also know as the relaxed TDM (\mathbf{Z}^{nm}) require the solution of a dynamic-polarizability-like equation,

$$|\mathbf{X}^{nm}, \mathbf{Y}^{nm}\rangle = -(\Lambda - \Omega_{nm}\Delta)^{-1} |P^{nm}, Q^{nm}\rangle \quad (\text{S27})$$

Explicit expressions for the right-hand-side (RHS) are provided in ref. 4, 7. However, within the adiabatic approximation to the exchange–correlation kernel, the linear response operator in Eq. S27 becomes singular when Ω_{nm} approaches any other excitation energy and thus the transition density diverges unphysically. [4, 7, 8] Detail about the calculation of relaxed TDM \mathbf{Z}^{nm} can be found in ref.4. In current implementation, we exclusively use derivative couplings from the pseudowavefunction approximation which is equivalent to ignoring the off-diagonal blocks of the TDM ($\mathbf{Z}^{nm} = 0$), and the TDM is parametrized as

$$\mathbf{T}^{nm} = \rho^{nm,PW} = \begin{pmatrix} \rho_{oo}^{nm,QR} & \mathbf{0} \\ \mathbf{0} & \rho_{vv}^{nm,QR} \end{pmatrix} \quad (\text{S28})$$

where the superscript *PW* and *QR* represent the pseudowavefunction and quadratic response, $\rho_{oo}^{nm,QR}$ and $\rho_{vv}^{nm,QR}$ are the occupied-occupied and virtual-virtual blocks of $\rho^{nm,QR}$, and \mathbf{T}^{nm} is referred to as the unrelaxed TDM. Based on the pseudowavefunction the Lagrange multiplier $\mathbf{D}^{nm} = \mathbf{T}^{nm}$ in Eq. 10 in our implementation.

Here, we borrow the shorthand definitions from ref.4

$$\mathbf{R}^{\pm n} = \mathbf{X}^n \pm \mathbf{Y}^n, \quad (\text{S29})$$

$$\mathbf{M}^{\pm} = \frac{1}{2}(\mathbf{M} \pm \mathbf{M}^T), \quad (\text{S30})$$

$$H_{pq}^{\pm n} = H_{pq}^{\pm}[\mathbf{R}^{\pm n}], \quad (\text{S31})$$

$$\bar{\Omega}_{nm} = \frac{1}{2}(\Omega_n + \Omega_m), \quad (\text{S32})$$

Now, the Lagrange energy-weighted transition density multiplier $\bar{\mathbf{W}}^{nm}$ based on the pseudowavefunction is determined as:

$$\begin{aligned} \bar{W}_{ij}^{+nm} &= \frac{1}{2}T_{ij}^{+nm} + \frac{1}{2}H_{ij}^{+}[\mathbf{D}^{nm}] + g_{ij}^{xc}[R^{+n}, R^{+m}] \\ &\quad - \frac{1}{4}\sum_a \varepsilon_a [R_{ia}^{+n}R_{ja}^{+m} + R_{ia}^{-n}R_{ja}^{-m} + (n \leftrightarrow m)] \\ &\quad + \frac{\bar{\Omega}_{nm}}{4}\sum_a [R_{ia}^{+n}R_{ja}^{-m} + R_{ia}^{-n}R_{ja}^{+m} + (n \leftrightarrow m)], \end{aligned} \quad (\text{S33})$$

$$\begin{aligned} \bar{W}_{ab}^{+nm} &= \frac{1}{2}T_{ab}^{+nm} + \frac{1}{4}\sum_i \varepsilon_i [R_{ia}^{+n}R_{ib}^{+m} + R_{ia}^{-n}R_{ib}^{-m} + (n \leftrightarrow m)] \\ &\quad + \frac{\bar{\Omega}_{nm}}{4}\sum_i [R_{ia}^{+n}R_{ib}^{-m} + R_{ia}^{-n}R_{ib}^{+m} + (n \leftrightarrow m)], \end{aligned} \quad (\text{S34})$$

$$\bar{W}_{ia}^{+nm} = \frac{1}{4} [H_{ji}^{+n}R_{ja}^{+m} + H_{ji}^{-n}R_{ja}^{-m} + (n \leftrightarrow m)], \quad (\text{S35})$$

$$\begin{aligned} \bar{W}_{ij}^{-nm} &= \frac{1}{2}T_{ij}^{-nm} + \frac{1}{2}H_{ij}^{-}[\mathbf{D}^{nm}] \\ &\quad - \frac{1}{4}\sum_a \varepsilon_a [R_{ia}^{+n}R_{ja}^{-m} + R_{ia}^{-n}R_{ja}^{+m} - (n \leftrightarrow m)] \\ &\quad + \frac{\bar{\Omega}_{nm}}{4}\sum_a [R_{ia}^{+n}R_{ja}^{+m} + R_{ia}^{-n}R_{ja}^{-m} - (n \leftrightarrow m)], \end{aligned} \quad (\text{S36})$$

$$\begin{aligned} \bar{W}_{ab}^{-nm} &= \frac{1}{2}T_{ab}^{-nm} + \frac{1}{2}H_{ab}^{-}[\mathbf{D}^{nm}] \\ &\quad + \frac{1}{4}\sum_i \varepsilon_i [R_{ia}^{+m}R_{ib}^{-n} + R_{ia}^{-m}R_{ib}^{+n} - (n \leftrightarrow m)] \\ &\quad + \frac{\bar{\Omega}_{nm}}{4}\sum_i [R_{ib}^{+n}R_{ia}^{-m} + R_{ib}^{-n}R_{ia}^{+m} - (n \leftrightarrow m)], \end{aligned} \quad (\text{S37})$$

$$\bar{W}_{ia}^{-nm} = \frac{1}{4} \left[H_{ji}^{+m} R_{ja}^{-n} + H_{ji}^{-m} R_{ja}^{+n} - (n \leftrightarrow m) \right], \quad (\text{S38})$$

where $(n \leftrightarrow m)$ signifies repeating the terms within the same bracket with n and m interchanged. Then, the generalized energy-weighted transition density in Eq. 10

$$\mathbf{W}^{nm} = \bar{\mathbf{W}}^{nm} - \frac{1}{4} \left[\mathbf{T}^{nm} + (\mathbf{T}^{nm})^T \right]. \quad (\text{S39})$$

Finally, the pair transition density in Eq. 10 is

$$\begin{aligned} \Gamma_{pqrs}^{nm} = & D_{pq}^0 D_{rs}^{nm} - c_x D_{ps}^0 D_{rq}^{nm} + 2R_{pq}^{+n} R_{rs}^{+m} \\ & + c_x \left[R_{pr}^{-n} R_{sq}^{-m} - R_{pr}^{+n} R_{sq}^{+m} - R_{pr}^{+n} R_{qs}^{+m} - R_{pr}^{-n} R_{qs}^{-m} \right], \end{aligned} \quad (\text{S40})$$

where $\mathbf{R}^{\pm n}$ should be interpreted as an occupied–virtual-only matrix and $D_{pq}^0 = \delta_{pi}\delta_{qi}$ is the ground state density matrix.

4. TESTING OF THE NON-ADIABATIC COUPLING CALCULATION

Comparisons between NAC vectors were conducted for both analytic and numerical implementations, which are very different methodologies. Analytical and numerical NACRs/NACTs for formaldimin (CH_2NH_2^+) and water (H_2O) computed with different exchange-correlation functionals (Hartree-Fock, PBE0, and B3LYP) are shown below. The NACT $\dot{\mathbf{R}} \cdot \mathbf{d}_{nm} = \langle \Psi_n | \frac{\partial}{\partial t} \Psi_m \rangle$ is a derivative relative to time, in which the NACR $\mathbf{d}_{nm}(\mathbf{R}) = \langle \Psi_n(\mathbf{r}, \mathbf{R}) | \nabla_{\mathbf{R}} \Psi_m(\mathbf{r}, \mathbf{R}) \rangle_{\mathbf{r}}$ is a derivative relative to position. Thus, NACR can calculate by numerical differentiation from the NACT. In practice, we manually displaced each atom along a Cartesian coordinate by 0.001 a.u. then update the CI vector and repay the NACT calculation to obtain each NACR element numerically. The following Figure S1 ~ S4 show the comparison of analytical NACR, numerical NACR, and NACT for formaldimine (CH_2NH_2^+) and water (H_2O) based on different exchange-correlation functional (pure Hartree-Fock, PBE0 and B3LYP). Since the NACT and analytical NACR calculation are very different methodologies. As expected, minor differences are observed between analytical and numerical implementations NACR since these involve different approximations. Such strong corresponding behavior among these quantities, especially the coincidental vector direction between analytical and numerical NACRs at the coupling moment, indirectly indicates the reliability of our implementation.

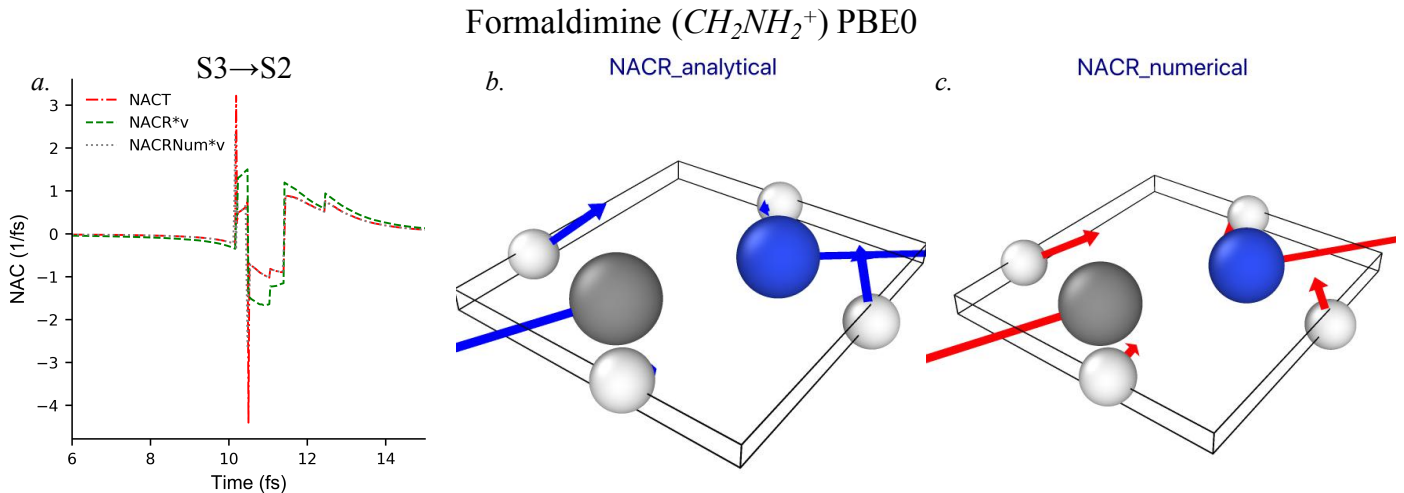


Fig. S1. Comparison of analytical NACR, numerical NACR and NACT in formaldimine with PBE0. *a.* Plot the coupling ($\dot{\mathbf{R}} \cdot \mathbf{d}_{nm}$) related to time for S3 to S2 hopping. *b.* and *c.* show the analytical NACR vectors and numerical NACR vectors at the S3 to S2 hopping moment.

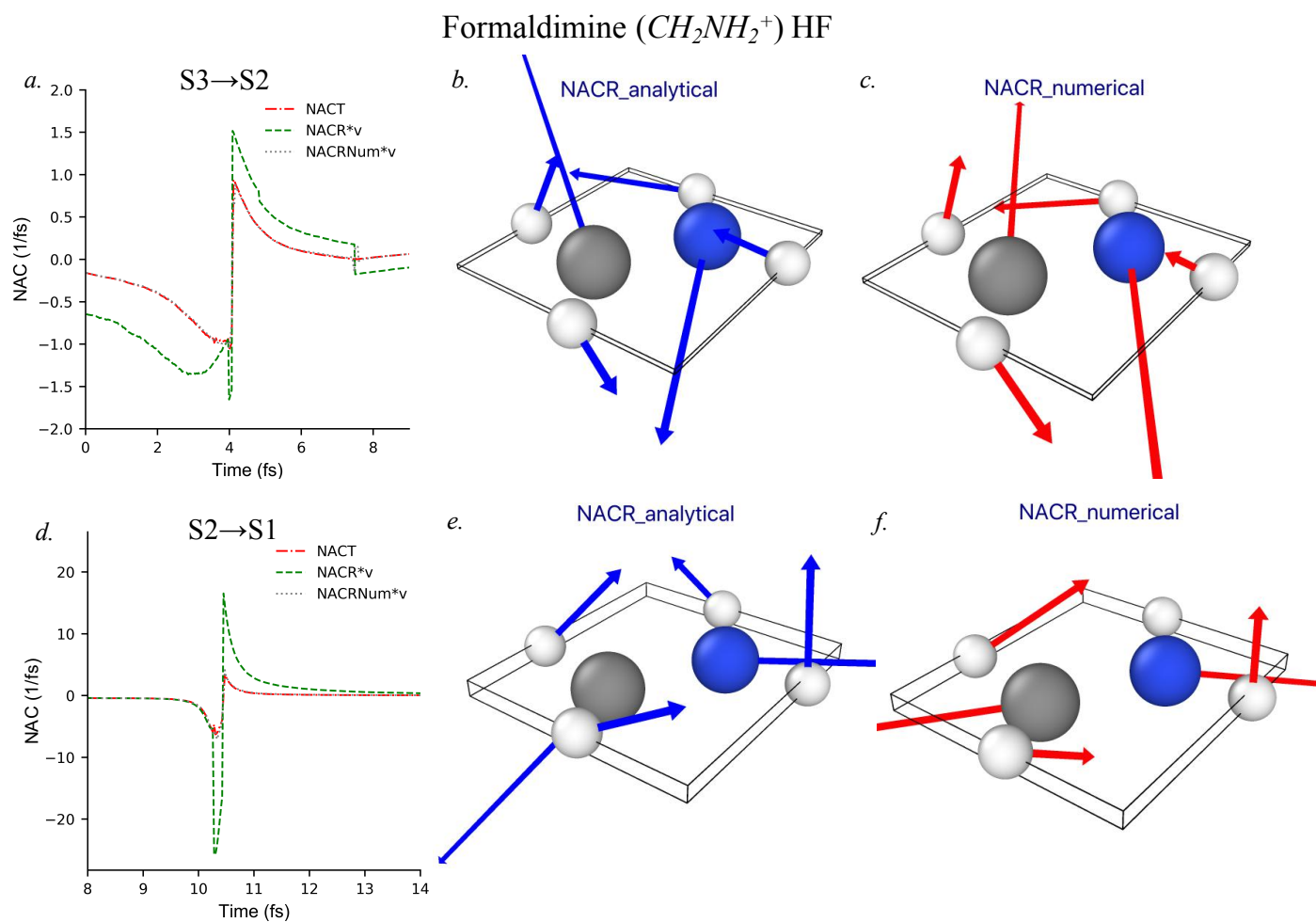


Fig. S2. Comparison of analytical NACR, numerical NACR and NACT in formaldimine with pure Hartree-Fock. *a.* Plot the coupling ($\vec{R} \cdot \mathbf{d}_{nm}$) related to time for S3 to S2 hopping. *b.* and *c.* show the analytical NACR vectors and numerical NACR vectors at the S3 to S2 hopping moment. *d.* is the profile of coupling at S2 to S1 hopping. *e.* and *f.* show the analytical NACR vectors and numerical NACR vectors at the hopping moment.

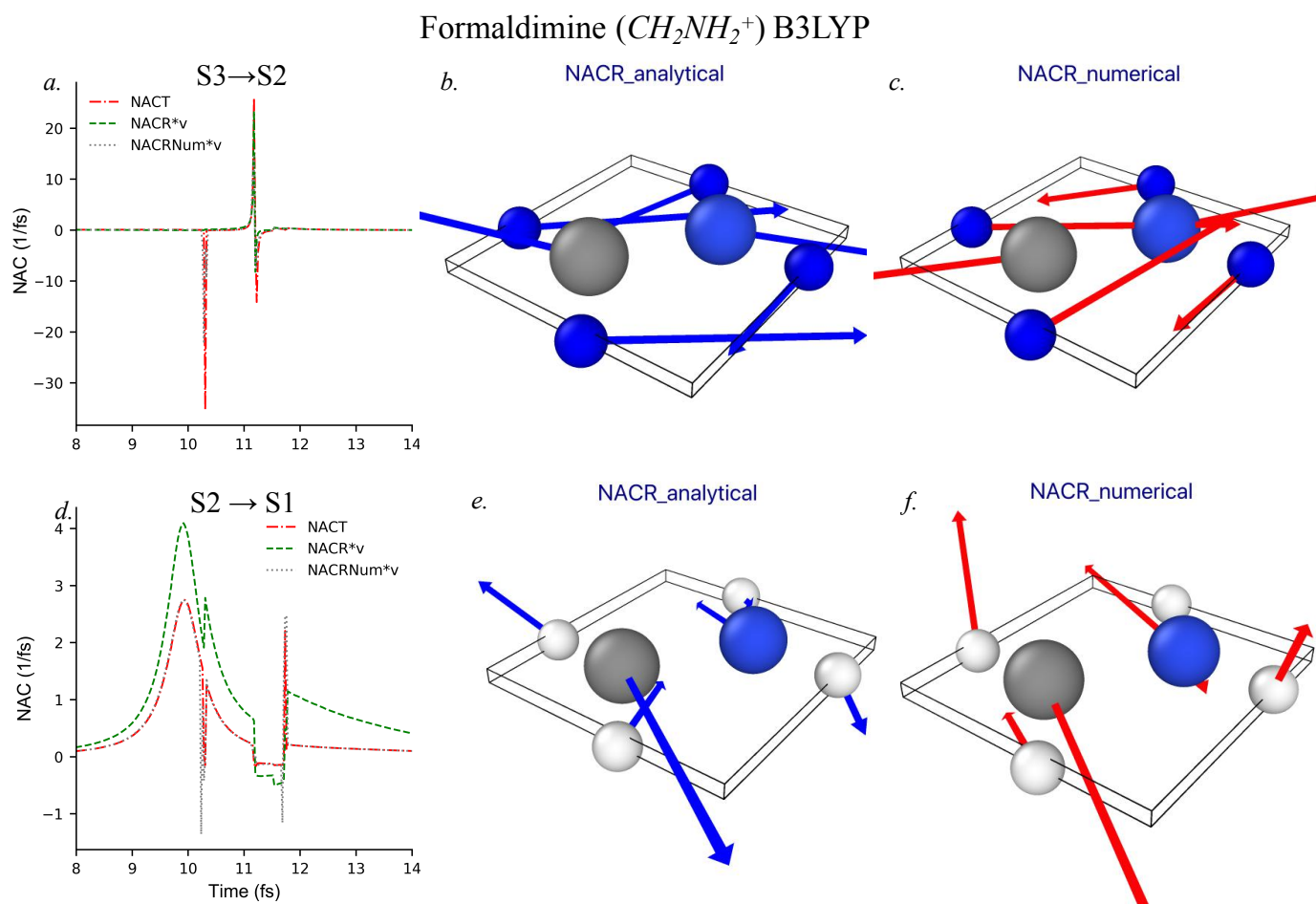


Fig. S3. Comparison of analytical NACR, numerical NACR and NACT in formalimine with B3LYP. *a.* Plot the coupling ($\dot{\mathbf{R}} \cdot \mathbf{d}_{nm}$) related to time for S3 to S2 hopping. *b.* and *c.* show the analytical NACR vectors and numerical NACR vectors at the S3 to S2 hopping moment. *d.* is the profile of coupling at S2 to S1 hopping. *e.* and *f.* show the analytical NACR vectors and numerical NACR vectors at the hopping moment.

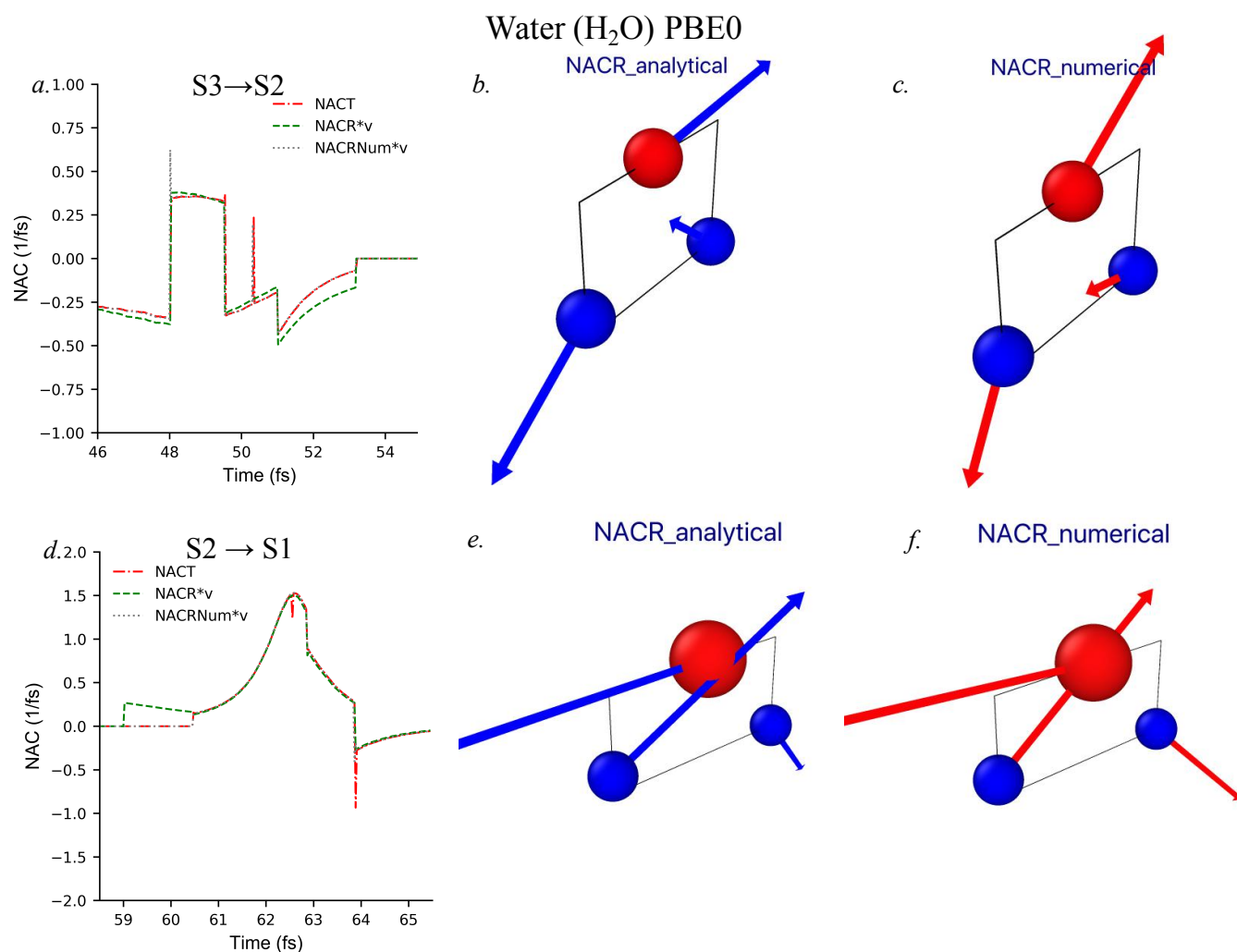


Fig. S4. Comparison of analytical NACR, numerical NACR and NACT in water with PBE0. *a.* plot the coupling ($\dot{\mathbf{R}} \cdot \mathbf{d}_{nm}$) related to time for S3 to S2 hopping. *b.* and *c.* show the analytical NACR vectors and numerical NACR vectors at the S3 to S2 hopping moment. *d.* is the profile of coupling at S2 to S1 hopping. *e.* and *f.* show the analytical NACR vectors and numerical NACR vectors at the hopping moment.

5. EXAMPLE NWCHEM INPUT

Example input file for FSSH calculation

```
start nwchem
echo

geometry
O  0.0000  0.0000  0.1197
H  0.0000  0.7615 -0.4790
H  0.0000 -0.7615 -0.4790
end

basis
* library 6-31G*
end

dft
xc b3lyp
end

tddft
nroots 10
notriplet
cis
civecs
grad
root 1
end
end

qmd
nstep_nucl 50
dt_nucl 0.5
targ_temp 300.0
thermostat svr 500
namd SH
nstates 5
init_state 3
dt_elec 0.1
decoherence IDC
end
end
task tddft qmd
```

In the namd sub-block within the qmd block, the keyword nstates sets the number of electronic states to include in the calculation, i.e. the number of states for use with Eq. 5. The number of roots requested in the tddft block must be at least nstates-1. The keyword init_state sets the initial electronic state to be occupied; the numbering for this keyword and the output that reports the currently occupied state runs from 0 (ground state) to nstates-1. So if you want to start a calculation in the first excited state, you would set init_state to 1. The keyword dt_elec sets the electronic time step for Eq. 5 (in atomic units). The nuclear time step (dt_nucl) must be an integer multiple of the electronic time step ($\text{mod}(\text{dt_nucl}, \text{dt_elec})=0$). The decoherence keyword selects which decoherence correction (IDC or EDC) should be used.

REFERENCES

1. F. Furche, "On the density matrix based approach to time-dependent density functional response theory," *J. Chem. Phys.* **114**, 5982–5992 (2001).
2. S. Tretiak and S. Mukamel, "Density matrix analysis and simulation of electronic excitations in conjugated and aggregated molecules," *Chem. Rev.* **102**, 3171–3212 (2002).
3. Q. Ou, G. D. Bellchambers, F. Furche, and J. E. Subotnik, "First-order derivative couplings between excited states from adiabatic TDDFT response theory," *J. Chem. Phys.* **142**, 064114 (2015).
4. S. Parker, S. Roy, and F. Furche, "Multistate hybrid time-dependent density functional theory with surface hopping accurately captures ultrafast thymine photodeactivation," *J. Chem. Theory. Comput.* **14**, 807–819 (2018).
5. F. Furche and R. Ahlrichs, "Adiabatic time-dependent density functional methods for excited state properties," *J. Chem. Phys.* **117**, 7433–7447 (2002).
6. I. Ryabinkin, J. Nagesh, and F. Izmaylov, "Fast numerical evaluation of time-derivative nonadiabatic couplings for mixed quantum-classical methods," *J. Phys. Chem. Lett.* **6**, 4200–4203 (2015).
7. S. Parker, D. Rappoport, and F. Furche, "Quadratic response properties from tddft: Trials and tribulations," *Phys. Chem. Chem. Phys.* **21**, 18999–19010 (2019).
8. S. Tretiak and V. Chernyak, "Resonant nonlinear polarizabilities in the time-dependent density functional theory," *J. Chem. Phys.* **119**, 8809–8823 (2003).